Article:
Coombes, J.D. orcid.org/0000-0002-5601-8977, Manka, P.P., Swiderska-Syn, M. et al. (21 more authors) (2025) Osteopontin Promotes Cholangiocyte Secretion of Chemokines to Support Macrophage Recruitment and Fibrosis in MASH. Liver International, 45 (4). e16131. ISSN 1478-3223

https://doi.org/10.1111/liv.16131

Liver INTERNATIONAL

Osteopontin promotes cholangiocyte secretion of chemokines to support macrophage recruitment and fibrosis in MASH.

Journal:	*Liver International*
Manuscript ID	LIVint-24-00576.R1
Wiley - Manuscript type:	Original Article
Date Submitted by the Author:	04-Sep-2024
Complete List of Authors:	Coombes, Jason D.; Foundation for Liver Research; King's College London Faculty of Life Sciences & Medicine; Saint Louis University School of Medicine P, Paul Manka; Foundation for Liver Research; King's College London Faculty of Life Sciences & Medicine; Ruhr-Universitat Bochum Swiderska-Syn, Marzena; Saint Louis University School of Medicine; University of Leeds Leeds Institute of Medical Research at St James's T, Danielle Vannan; University of Calgary Calvin Phoebe and Joan Snyder Institute for Chronic Diseases; University of Calgary Riva, Antonio; Foundation for Liver Research; King's College London Faculty of Life Sciences & Medicine C, Lee Claridge; Leeds Teaching Hospitals NHS Trust Moylan, Cynthia; Duke University Division of Gastroenterology Suzuki, Ayako; Duke University Division of Gastroenterology A, Marco Briones-Orta; Foundation for Liver Research; King's College London Faculty of Life Sciences & Medicine Younis, Rasha; Foundation for Liver Research Kitamura, Naoto; Foundation for Liver Research Sydor, Svenja; Ruhr-Universitat Bochum Bitencourt, Shanna; Vrije Universiteit Brussel Mi, Zhiyong; University of South Florida Kuo, Paul C.; University of South Florida Diehl, Anna Mae; Duke University Division of Gastroenterology van Grunsven, Leo; Vrije Universiteit Brussel Chokshi, Shilpa; Foundation for Liver Research; King's College London Faculty of Life Sciences & Medicine Canbay, Ali; Ruhr-Universitat Bochum Abdelmalek, Manal F.; Mayo Clinic Division of Gastroenterology and Hepatology Aspichueta, Patricia; Universidad del Pais Vasco Papa, Salvatore; University of Leeds Leeds Institute of Medical Research at St James's Eksteen, Bertus; University of Calgary Calvin Phoebe and Joan Snyder Institute for Chronic Diseases; University of Calgary Syn, Wing-Kin; Foundation for Liver Research; Saint Louis University School of Medicine; Universidad del Pais Vasco
Manuscript Topic:	Nonalcoholic Fatty Liver Disease
Keywords:	Osteopontin, Chemokine, Cholangiocyte, Macrophage, NASH, Fibrosis

Title Pages

Osteopontin promotes cholangiocyte secretion of chemokines to support macrophage recruitment and fibrosis in MASH.

Authors:

Jason D. Coombes[1,2,14], Paul P Manka[1,2,3], Marzena Swiderska-Syn[13], Danielle T Vannan[5,6], Antonio Riva[2,7], Lee C Claridge[8], Cynthia Moylan[4], Ayako Suzuki[4], Marco A Briones-Orta[1,2], Rasha Younis[1], Naoto Kitamura[1], Svenja Sydor[3], Shanna Bittencourt[10], Zhiyong Mi[9], Paul C. Kuo[9], Anna Mae Diehl[4], Leo A van Grunsven[10], Shilpa Chokshi[2,7], Ali Canbay[3], Manal F. Abdelmalek[11], Patricia Aspichueta[12], Salvatore Papa[13], Bertus Eksteen[5,6], Wing-Kin Syn[1,12,14]

[1] Regeneration and Repair, Institute of Hepatology, Foundation for Liver Research, London, United Kingdom.

[2] Faculty of Life Sciences and Medicine, King's College London, London, United Kingdom.

[3] Gastroenterology and Hepatology, University Clinic Bochum, Bochum, Germany.

[4] Division of Gastroenterology, Department of Medicine, Duke University, Durham, North Carolina.

[5] Snyder Institute for Chronic Diseases, University of Calgary, Alberta, Canada.

[6] Aspen Woods Clinic, Calgary, Alberta, Canada

[7] Viral Hepatitis and Alcohol Research Group, Institute of Hepatology, Foundation for Liver Research, London, United Kingdom.

[8] Department of Hepatology, Leeds Teaching Hospital NHS Trust, UK.

[9] Department of Surgery, University of South Florida, Tampa, Florida.

[10] Liver Cell Biology, Vrije Universiteit, Brussels, Belgium.

[11] Division of Gastroenterology and Hepatology, Mayo Clinic, Rochester, Minnesota.

[12] Department of Physiology, Faculty of Medicine and Nursing, University of the Basque Country, EPV/EHU, Leioa.

[13] Leeds Institute of Medical Research, St. James's University Hospital, University of Leeds, Leeds, UK.

[14] Division of Gastroenterology and Hepatology, School of Medicine, Saint Louis University, Saint Louis, Missouri, USA.

Corresponding Author: Wing-Kin Syn, MD PhD, Division of Gastroenterology and Hepatology, Saint Louis University School of Medicine. wingkin.syn@health.slu.edu

Financial Support:

This study was funded predominantly by CORE-UK (WKS), BRET (WKS), EASL (WKS, PPM), The Foundation for Liver Research London (WKS, SC), the University of Birmingham (WKS), and GASL (PPM). Additional funding was provided by the National Institute of Health R01 DK077794 (AMD), Belgian Federal Science Policy Office (Interuniversity Attraction Poles program - P6/20 and P7/83-HEPRO) (LvG), the Brussels Capital Region (INNOVIRIS Impulse programme-Life Sciences 2007 and 2011; BruStem) (LvG), the Institute for the Promotion of Innovation through Science and Technology in Flanders (SBO-IWT-090066 HEPSTEM) (LvG), the Natural Sciences and Engineering Research Council of Canada Postgraduate Doctoral Scholarship (BE), the Alberta Innovates Technology Futures Graduate Scholarship (BE), DFG (German Research Association) CA267/8-1 (AC), and the Wilhelm Lapitz Foundation (AC).

Disclosures: None declared.

Abbreviations:

CLD, Chronic liver disease

CCL, Chemokine (C-C motif) ligand

CCR, CC chemokine receptors

CD, Cluster of differentiation

CXCL, Chemokine (C-X-C motif) ligand

HSC, Hepatic stellate cell

LPC, Liver progenitor cell

Ly6c, Lymphocyte antigen 6 complex

MAFLD, metabolic dysfunction-associated fatty liver disease

MASH, metabolic dysfunction-associated alcoholic steatohepatitis

OPN, Osteopontin

Acknowledgements:

Dr. G. J. Gores (Mayo Clinic, Rochester, MN) and Yoshiyuki Ueno (Tohoku University, Sendai, Japan) for providing the murine immature ductular cell line (603B). Karine Vanacker and Frederic Flamant (IGSL, Lyon), Benjamin Gillet and Sandrine Hughes (PSI, IGSL) for supplying materials and assistance with RNA sequencing.

ABSTRACT

Background and aims

Osteopontin (OPN) promotes the ductular reaction and is a major driver of chronic liver disease (CLD) progression. Although CLD is characterized by the accumulation of inflammatory cells including macrophages around the peri-portal regions, the influence of OPN on recruitment is unclear. We investigated the role of OPN in cholangiocyte chemokine production and macrophage recruitment by combining *in vivo*, *in vitro*, and *in silico* approaches.

Methods

The effects of OPN on cholangiocyte chemokine production and macrophage migration were assessed in culture, alongside RNA-sequencing to identify genes and pathways affected by OPN depletion. Murine liver injury models were used to assess liver chemokine expression and liver macrophage/monocyte recruitment. OPN and chemokine expression were analysed in liver tissue and plasma from biopsy-proven MASH patients.

Results

OPN-knockdown in cholangiocytes reduced chemokine secretion. RNA-sequencing showed OPN-related effects clustered around immunity, chemotaxis and chemokine production. Macrophage exposure to cholangiocyte-conditioned media showed OPN supported migration via chemokines CCL2, CCL5 and CXCL1. These effects were related to NF-κB signalling. Murine liver fibrosis was accompanied by upregulated liver OPN, CCL2, CCL5, and CXCL1 mRNA, and accumulation of liver CD11b/F4/80^{+}CCR2^{high} macrophages but treatment with OPN-specific neutralizing aptamers reduced fibrosis, chemokine mRNAs and accumulation of liver CD11b/F4/80^{+}CCR2^{high}/ Ly6C^{high} inflammatory monocytes. In human MASH, liver OPN correlated with chemokines CCL2 and IL8 in association with portal injury and fibrosis. Plasma OPN, serum CCL2 and IL8 also increased with fibrosis stage.

Conclusions

OPN promotes cholangiocyte chemokine secretion and the accumulation of pro-inflammatory monocytes. These data support neutralization of OPN as an anti-inflammatory and anti-fibrotic strategy.

[249 words]

Keywords

Osteopontin, Chemokine, Cholangiocyte, Macrophage, MASH, Fibrosis.

INTRODUCTION

Despite considerable progress towards understanding the cellular and inflammatory factors that drive chronic liver disease (CLD) progression, specific therapies that ameliorate CLD still elude clinical translation. Targeting liver fibrosis, the most predictive indicator of disease progression and negative prognosis would present attractive modalities for therapeutic intervention [1,2].

We have reported that Osteopontin (OPN) is a key driver of liver fibrogenesis via activation of hepatic stellate cells (HSCs) and progenitor cells [3]. OPN mediates crosstalk between periportal and stromal cells and drives the ductular reaction which is highly linked to fibrogenesis [3,4]. An acidic member of the small integrin-binding ligand N-linked glycoprotein (SIBLING) family of proteins, OPN is abundantly expressed in a wide range of tissues during inflammation and repair. It is secreted by various cell-types including epithelial cells, T cells, dendritic cells and macrophages, and its expression is induced by oxidative stress, growth factors (e.g. PDGF, TGFβ), and cytokines (e.g. IL6, TNFα). In normal liver, OPN is expressed by cholangiocytes, HSCs, progenitors, and immune cells (macrophages, DCs, B and T cell subsets). To date, OPN has been shown to be upregulated in human CLD (viral hepatitis B and C, NAFLD/MAFLD, ALD, PBC, PSC, autoimmune hepatitis) and in models of liver injury (bile-duct ligation, biliary fibrosis; methionine-choline deficient diet (MCD), MASH-fibrosis; carbon tetrachloride injection (CCl_4), fibrosis). Liver and serum/plasma OPN levels correlate with severity of liver fibrosis in humans and mice [5].

A specific role for OPN in macrophage activation and recruitment in CLD, however, remains unclear. In liver, inflammatory monocytes, particularly myeloid-derived macrophages, influence pro-inflammatory and pro-fibrotic progression and through crosstalk maintain HSC activation [6]. Interestingly, depending on macrophage *subset* as defined by activation

markers, there also appears to be a key role in resolving fibroinflammatory disease in murine CLD models [7]. CD11b^{high}F4/80^{int}Ly6C^{high} infiltrating monocyte-derived macrophages accumulate early in disease to promote fibrosis whereas CD11b^{high} F4/80^{int}Ly6C$^{int//low}$ macrophages regulate fibrosis resolution by the expression of more MMPs.

As the nature of the inflammatory response appears to influence the course and outcome of CLD, directing therapy at the recruitment of subsets and/or signals involved could attenuate liver injury and fibrosis. Furthermore, portal fibrosis has been shown to be the best predictor of liver complications during follow-up [8]. Previous work has indicated that inflammatory cell accumulation in portal tracts is influenced by activated-HSC derived Hedgehog (Hh) ligands, which induce cholangiocytes to secrete chemokines including CXCL16 and thereby recruit inflammatory NKT cells [9]. Hh signals drive OPN production and this mechanism of inflammatory recruitment is shown to drive fibrogenesis [5]. Additionally, we have reported that the greatest levels of OPN expression in the injured liver are in the periportal regions, and in colocation with the cholangiocyte marker Keratin 19 [3]. We therefore sought to investigate whether OPN modulates cholangiocyte chemokine secretion that leads to macrophage recruitment.

We have combined multiple investigatory disciplines, including human data, multiple animal models, cell culture and bioinformatic analysis of next-generation gene sequencing. We find that OPN critically affects cholangiocyte chemokine secretion to promote macrophage recruitment in CLD and moreover may promote an inflammatory response that favours fibrosis progression.

EXPERIMENTAL PROCEDURES

Cellular analyses

The murine cholangiocyte cell line 603B and murine macrophage line RAW264.7 were maintained according to standard protocols [10,11]. For migration experiments, 603B-conditioned media was transferred to the bottom chamber of a standard transwell apparatus (Nunc, ThermoFisher, Paisley, UK); RAW264.7 were seeded into the top chamber on a polycarbonate membrane with 8 um pores. Migrated cells were counted using coomassie blue staining of cells translocated to the underside of the membrane, using at least 15 nonoverlapping fields from two independent experiments.

Stable OPN knockdown using short-hairpin RNA was achieved as described [3]. OPN knockdown 603B cells (shOPN-603B) were compared with non-targeting scrambled shRNA (shScr-603B). For select experiments, conditioned media was treated with either OPN-neutralizing aptamer ("OPN Apt", versus sham control aptamer "Sham Apt"), recombinant OPN (rOPN, 100 ng/mL, R&D), OPN-neutralizing antibody (2 ug/ mL R&D) neutralizing antibodies against CCL2, CXCL1, CCL5 or control IgG (3 µg/mL; 0.5 ug/uL; 0.5 ug/uL and 3 ug/mL, respectively).

Molecular RNA Sequencing and bioinformatics analyses

RNA was collected from snap-frozen 603B cell pellets ($2x10^6$ cells) using a standard Trizol protocol. RNA sequencing was performed on an Ion Proton™ (Life Technologies) Next Generation Sequencing platform (at the Institut de Génomique Fonctionnelle, Lyon, France). The Htseq software [12] count feature (Reserve strand setting) was used to map reads (Bam files) on UCSC mouse genome release Mm10 and generate count tables. The Deseq2 R package from Bioconductor was used to analyze each count table separately [13]. Only genes

exceeding a conservative threshold of at least 10 reads in one sample were kept (considered to be expressed; False discovery rate 0.05). Selected genes were considered "Called Differential" if they satisfied a Benjamini-Hochsberg [14] p-adjusted value <0.05 and had Log2-fold change either >1 or <-1. Gene ontologies and functional enrichment were analysed using two modalities: GOrilla [15,16] and DAVID [17,18] software. Multiple GO terms were synthesized in ReviGO to simplify functional categories and reduce redundancy [19]. Specific altered pathways detected from RNA-Seq data were generated from the KEGG database [20,21].

Animal models

Mice were housed in 12-hr light/dark cycle with food and water ad libitum. Liver samples for RNA analyses and immunohistochemistry were taken at the indicated timepoints. Animal handling was conducted in line with the US National Research Council's Guide for the Care and Use of Laboratory Animals, the US Public Health Service's Policy on Humane Care and Use of Laboratory Animals, the UK Animals (Scientific Procedures) Act 1986 Amendment Regulations (SI 2012/3039), and European Union Directive 2010/63/EU with approval by the relevant institutional committees of Duke University; Vrije Universiteit Brussel, Belgium; University of Calgary, Canada.

Murine Methionine-choline deficient diet (MCD), 3,5,-Diethoxycarbonyl-1,4-dihydrocollidine diet (DDC) and Carbon tetrachloride (CCl_4) models were performed as described [3]. MCD mice (n=5/group) were fed methionine-choline deficient (MCD) diet or control chow for 5 weeks to induce metabolic dysfunction-associated steatohepatitis (MASH) fibrosis. CCl_4 mice (n=5/group) received twice-weekly intraperitoneal injections of CCl_4 (0.5

mg/kg, Sigma-Aldrich) or vehicle (mineral oil) for 6 weeks. DDC mice (n=5/group) were fed the dihydrocollidine (DDC) diet for 3 weeks to induce biliary-type fibrosis.

OPN neutralization

Mice received OPN-specific aptamers (specifically neutralize circulating-extracellular OPN) or sham-aptamers (negative control) [22,23] by tail-vein injections in the final week of dietary or chemical challenge (n=10/study; 5/group; four injections (alternate days) total per mouse; 200 μg in 100 μL of PBS). Mice were sacrificed 24 h after the final aptamer dose.

Histology and Immunohistochemistry

Liver tissue was formalin-fixed, paraffin-embedded, and cut into 5-μm sections. To quantify liver fibrosis, five-micron sections were stained with picrosirius red (Sigma, St. Louis, MO) and counterstained with fast green (Sigma, St. Louis, MO). Immunohistochemical staining was performed as previously described [3] to detect OPN, αSMA, F4/80, CD68 and Cytokeratin 19 (CK19) using procedures described in ***Supplemental Methods***.

Human Histology and tissue analyses

Studies using human material from Duke University Hospital were conducted in accordance with NIH and Institutional guidelines for human subject research and the Declaration of Helsinki (2008). For formalin-fixed, paraffin-embedded (FFPE) sections, deidentified samples were obtained from explanted liver tissue from individuals undergoing transplantation for MASH-cirrhosis, and normal tissues were obtained from excess split-liver grafts. Total liver RNA was obtained from freshly explanted and snap-frozen MASH.

Biobanked samples (Duke NAFLD/MAFLD repository) were collected on same day as acquired liver histology.

Tissue Microarray and Luminex cytokine profile

Transcriptomic data was generated from frozen liver biopsy tissue obtained from patients previously enrolled in the Duke University Health System NAFLD/MAFLD Biorepository. Clinically-indicated liver biopsies and liver histology were graded and scored for MAFLD-related injury and fibrosis according to published criteria [24]. Transcriptomic data from 72 patients was analysed, including 40 with mild MAFLD, defined as fibrosis stages 0 or 1, and 32 with severe MAFLD, defined as fibrosis stages 3 or 4. The biorepository, patient demographics, RNA preparation and generation of genomic data have been described previously [25]. Briefly, microarray hybridization was performed using Affymetrix Human Genome U133 Plus 2.0 GeneChip arrays (Affymetrix, Santa Clara, CA). Differential gene expression for *CXCL8*, *CCL2* and *SPP1* was determined using two sample Student's t-test assuming equal variances (Matlab, Mathworks, Natick, MA). Cytokine profiling was performed on biobanked serum and plasma samples (123 patients) using a Luminex analyte panel according to manufacturer's instructions (and **Supplemental methods**).

Protein detection and gene expression

Semiquantitative real-time PCR (qRT-PCR), western blotting and agarose gel electrophoresis were performed as described in **Supplemental methods.** NF-κB activity and specific subunit was detected using TransAM® NFκB p50, p52, p65 & Family Kits (Active Motif, Carlsbad, CA). Chemokines secreted in culture were measured by cytometric bead array (BD

Biosciences, Oxford, UK). ELISA detection of secreted OPN in media was performed as per kit manufacturer instructions (R&D Systems, Abingdon, UK).

Statistical analyses

For groupwise comparisons, analyses were performed using Graph-Pad Prism 4 software (GraphPad Software, La Jolla, CA) and data presented as mean±SEM. For two independent groups unpaired t-test was used with Welch correction to tolerate unequal variances, and for multiple comparisons a one-way ANOVA with Tukey's MCT post-hoc correction. Statistically significant differences were considered at $p \leq 0.05$.

RESULTS

Osteopontin is associated with chemokine production by cholangiocytes

The role of OPN in cholangiocyte chemokine secretion was investigated in vitro using the 603B cell line, which highly expresses both OPN and the cholangiocyte/ductular marker keratin 19 (**Figure 1A**) and secretes a copious amount of OPN as detected by ELISA of conditioned media (**Figure 1B**). Knockdown of OPN using lentivirus-mediated short-hairpin RNA targeting Osteopontin (shOPN) achieved approximately 65% knockdown versus non-targeting scrambled control (shScr) (**Figure 1C**) (Western quantitation shown in **Supplemental Figure 7**). We initially examined *production* of selected chemokines CCL2 (MCP-1), CXCL1 (KC/FSP/Gro1) and CCL5 (RANTES) and found that knockdown of OPN was associated with significantly downregulated mRNA of these chemokines (80%, 40% and 95% downregulation, respectively) (**Figure 1D**). Similar reductions were found for *secretion* of these chemokines, as detected by cytometric bead array examination of 603B conditioned media (approx. 75%, 60% and 85% loss of secretion, respectively) (**Figure 1E**).

To gain a wider appreciation of all the chemokines that may be affected and to investigate the wide array of signalling processes that could affect chemokine production in relation to OPN, we applied Next Generation RNA Sequencing (RNAseq). Appreciable levels of transcript were detected in 11,728 genes. Among these, we determined 670 genes to be significantly altered (Benjamini-Hochsberg p_{adj} <0.05), of which 192 genes were altered by more than 1x log_2Fold, a conservative cutoff which may underline functionally significant downregulation. Among these significantly altered genes, many of the most highly altered were chemokines (listed in **Table 1**). We detected alterations in 17 chemokines, of which 14/17 were downregulated, 10 by more than 1xlog_2fold and with statistical significance. In addition to aforementioned CCL2, CXCL1 and CCL5, significantly downregulated chemokines included

CXCL16, CXCL11, CXCL10, CCL9, CCL7, CX3CL1 (Fractalkine) and CXCL5. To account for the possibility of error associated with the high-throughput RNAseq process we independently verified these chemokines using qRT-PCR, which showed similarly consistent levels (***Supplemental Figure 1***), indicating the accuracy of the RNAseq and the robustness of chemokine downregulation.

The functional significance of the full range of altered genes detected by RNAseq was interrogated using Gene Ontology (GO) analysis to identify the most strongly-represented functional clusters among the differentially expressed genes. Two different modalities, GOrilla software and DAVID software, provided remarkably similar results (**Supplemental Table 3**). The enriched terms heavily favoured *chemokine and immune cell recruitment functional terms*, especially among the most significant hits, implying a role for OPN in these processes. The predominance of these terms also supports the primacy of these functions in relation to OPN i.e., the main function of OPN in cholangiocytes appears to be highly related to chemokine production and signals for chemotaxis/immune recruitment. A synthesis of all GO terms reported by GOrilla using ReviGO software to sort functional groupings also demonstrates that overwhelmingly the largest effect of OPN was on immune/inflammatory recruitment and chemokine/cytokine production (***Supplemental Figure 2***). Additionally, interrogation of altered genes via the KEGG signalling database indicated a robust role for OPN in chemokine/cytokine production and immune recruitment signalling pathways, which were the predominantly represented pathways (**Supplemental Table 4**).

OPN promotes non-canonical NF-κB signalling in cholangiocytes

Some affected GO terms were related to NF-κB signalling, which is known to be one of the main pathways for chemokine production and is also associated with activation by OPN. We

therefore investigated whether OPN was driving NF-κB activity in cholangiocytes. NF-κB activity assays showed that loss of OPN in 603B was associated with suppression of the *non-canonical* NF-κB pathway (repression of p52 and RelB activity in shOPN relative to shNS), but not the canonical branch (there was no suppression of p50, c-Rel, or p65 activity) (**Figure 2**). This implies that OPN stimulates a non-canonical NF-κB signalling mechanism in cholangiocytes. Searching the RNAseq data for known NF-κB-responsive *target* genes, aside from the chemokines identified already, indicates 25 target genes were significantly altered in shOPN cholangiocytes (Benjamini-Hochsberg p_{adj} <0.05); 24 out of these 25 genes were *downregulated* and 12 out of these 25 by more than 1 $\log_2$fold (***Supplemental Table 5***). Three NF-κB-family genes were also downregulated: *Nfkbid* ($I\kappa B_{NS}$, atypical IκB protein, modulator of nuclear NF-κB function), *Nfkbia* (IκBα, canonical inhibitor of NF-κB) and *Nfkb2* (NF-κB p100 subunit).

OPN enhances cholangiocyte-associated macrophage migration

To explore whether this deficiency in chemokine production affected macrophage recruitment we treated RAW264.7 macrophages with conditioned media from 603B cholangiocytes. 603B-conditioned media stimulated macrophage migration across transwell membranes (**Figure 3A**), however macrophage migration was comparably reduced with conditioned media from shOPN cholangiocytes (**Figure 3C**). Furthermore, neutralizing the chemokines CCL2, CXCL1 and CCL5 (using neutralizing antibodies; **Figure 3A**) abrogated transmigration in comparison to wildtype cholangiocyte conditioned media treated with non-specific IgG-control. Neutralization of OPN by antibody or by aptamer similarly reduced macrophage transmigration, whereas spiking the conditioned media with recombinant OPN (rOPN) enhanced migration (**Figures 3A, 3B**). These results indicate that OPN can directly

enhance cholangiocyte-stimulated macrophage migration, but also *indirectly* instruct the recruitment capacity of cholangiocytes by influencing the chemokine composition of the cholangiocyte secretome. The activation phenotype of macrophages also appears to be affected, as knockdown of OPN in 603B was associated with decreased expression of the inflammatory activation marker CIITA and increased expression of the immunomodulatory/resolving activation marker Arg1 (**Figure 3D**).

OPN neutralization inhibits inflammatory monocyte accumulation and chemokine expression in mouse models of liver injury.

To investigate whether the influence of OPN on inflammatory monocyte accumulation extends to the *in vivo* context we studied murine models of liver injury and fibrosis. We used an interventional approach, whereby circulating OPN was targeted by specific neutralizing-aptamer treatment in the MCD dietary model and the CCl_4 toxicity model. Additionally, biliary-type fibrosis was modelled using the DDC diet. We have previously shown the aptamer neutralization modality to be effective in these murine models and comparable to a neutralizing antibody modality [3].

MCD model. Consistent with our previous reports [3,26], in a 5-week MCD model, mice treated with Osteopontin-neutralizing aptamer had approximately 50% reductions in ALT, which would be in line with reduced inflammation. Simultaneously, fibrogenesis and HSC activation was also ameliorated (whole liver tissue *aSMA* mRNA by 2.1-fold; *Col1a1* mRNA by 2.2-fold; **Figure 4A**). Sirius red histology also demonstrated markedly reduced fibrosis with OPN neutralization (**Figure 4B**). Moreover, consistent with the *in vitro* findings, the induction of chemokines CCL2, CXCL1 and CCL5 was significantly ameliorated by OPN neutralization (whole liver tissue mRNA; **Figure 4C**).

CCl_4 model. Similar results were present in the 6-week CCl_4 model. The reductions in fibrogenesis (*aSMA* and *Col1a1)*, as we have previously reported with OPN-neutralizing aptamer treatment in the CCl_4 model [3], and reductions in collagen-rich fibrotic matrix were accompanied by significant reductions in chemokine mRNA, whereby the induction of CCL2, CXCL1 and CCL5 was almost completely reversed by OPN neutralization (**Figure 4C**).

DDC model. As a model of biliary-type fibrosis, we used a 3-week DDC model with 1.5 weeks OPN aptamer treatment. Consistent with the MCD and CCl_4 models, OPN neutralization was associated with significantly reduced levels of chemokines CCL2, CXCL1 and CCL5 (whole tissue mRNA; ***Supplemental Figure 4***).

Inflammatory cell recruitment. The presence of inflammatory cell recruitment was assessed using immunohistochemical detection of the F4/80 marker. Chronic liver injury is typically associated with accumulation of F4/80-positive cells, particularly around periportal regions (**Figure 5A**). In the MCD model, this accumulation was significantly reduced in mice treated with OPN neutralization. Flow cytometry of homogenized whole liver tissue was also used to detect inflammatory monocytes. In a supplemental study using a neutralizing antibody modality, OPN neutralization resulted in a 23% reduction in the accumulation of $CD11b^{high}F4/80^{high}$ inflammatory monocytes (***Supplemental Figure 5***).

Due to marked heterogeneity among inflammatory monocyte subsets, we sought to functionally characterize differences in accumulation influenced by OPN. In other murine studies, it has been shown that $CD11b^{high}F4/80^{int}Ly6C^{high}$ infiltrating monocyte-derived macrophages accumulate early in disease to promote fibrosis whereas $CD11b^{high}F4/80^{int}Ly6C^{int/low}$ macrophages regulate fibrosis resolution by expressing more

MMPs [7]. Notably, we find that OPN neutralization is also associated with reduced accumulation of the CD11b^{high}F4/80^{int}Ly6C^{high} subset (5.3% vs 1.6% of cells gated on CD11b^{+}F4/80^{+}) associated with inflammation and maintenance of fibrosis. Additionally, the CD11b^{high}F4/80^{int}Ly6C$^{int/low}$ population (associated with fibrosis resolution) was increased with OPN neutralization (**Figure 5B**). Altogether, these combined data indicate that *OPN supports inflammatory monocyte recruitment, particularly a profibrotic subset*. Furthermore, these data are consistent with OPN neutralization as a modality to suppress the pro-inflammatory monocyte activity that maintains fibrosis.

OPN and chemokine expression is associated with portal injury and fibrosis in human MASH

Immunohistochemical detection of the macrophage marker CD68 indicates a marked accumulation in MASH patients compared with normal liver (**Figure 6A**). This was particularly evident in portal regions, in close proximity to cholangiocytes. Dual-immunohistochemistry was performed to observe co-localisation of OPN with cholangiocytes (CK19 marker). There was a very apparent colocalization of CK19 and OPN (**Figure 6C**). with a high degree of cellular coexpression. Coexpression increased significantly in MASH vs normal liver, consistent with a regulatory role of OPN.

Portal inflammation and portal fibrosis have been shown to have consistent histological association with advanced MAFLD [27]. Our analysis of a luminex cytokine profile of 123 histologically evaluated MAFLD patients indicated significant associations with histological features of MASH. Specifically, between serum OPN and both *portal inflammation* and *portal fibrosis* (p=0.0006, positive; p=0.0008, positive; Spearman Rho.), Additionally, chemokines CCL2 and IL-8 (human functional equivalent of murine CXCL1/KC) also

positively correlated with both *portal inflammation* (p=0.0012 and p=0.038, respectively) and *portal fibrosis* (p=0.0025 and p=0.0001, respectively) (**Supplemental Table 6**).

In a separate analysis, OPN and chemokine expression was further explored in the context of fibrosis severity. Transcriptomic data was generated from biopsies of MASH histologically-proven and staged patients (*n*=72; 40 mild MAFLD, defined as fibrosis stage 0 or 1; 32 severe MAFLD, defined as fibrosis stage 3 or 4) using Affymetrix Human Genome U133 Plus 2.0 GeneChip microarrays. Chemokines CCL2 and IL8 were upregulated (approximately 50% and 140%, respectively) in livers with *advanced* MASH (i.e. *advanced fibrosis*) vs. *early* MASH (i.e. *early fibrosis*), while OPN was similarly increased from early to advanced MASH (approximately 175%) (**Figure 6B**).

DISCUSSION

We report that OPN drives chemokine production in cholangiocytes, which serves to recruit inflammatory monocytes / macrophages in chronic liver injury. Loss of OPN was associated with markedly reduced expression and secretion of a range of chemokines including CCL2, CXCL1 and CCL5 among others. This was associated with OPN-related stimulation of NF-κB signalling. Of novel importance, this was not via the canonical branch of the pathway, but via non-canonical NF-κB involvement. Additionally, OPN enhances cholangiocyte associated macrophage migration by both indirect and direct effects. Moreover, in murine models of chronic injury, OPN *neutralization* was associated with reduced accumulation of inflammatory monocytes ($F4/80^{+}$). The presence of OPN supported the recruitment of *profibrogenic* subpopulations (murine $Ly6C^{high}$), whereas OPN neutralization was associated with loss of chemokine secretion and the relative accumulation of a fibrosis resolution-associated subpopulation ($Ly6C^{low}$). Together, these data suggest that, in the liver, OPN is a

key driver of inflammatory macrophage recruitment via modulation of cholangiocyte chemokine expression and non-canonical NF-κB signalling.

The association of OPN with portal inflammation and fibrosis in human MASH, and indeed with worsening MASH is consistent with previous observations that OPN drives the ductular response [3] and is a regulator of immune recruitment [5] to facilitate fibrosis. The ductular reaction is recognised as a key determinant of progressive fibrosis in patients with MASH [28]. Furthermore, portal macrophage activity is specifically associated with the ductular reaction and fibrosis progression in CLD [29]. Targeting a molecular determinant of portal macrophage recruitment, especially one that promotes fibrosis, would be a critical avenue to intervene in fibrosis progression and halt worsening MASH. We have previously demonstrated that OPN neutralization is a viable strategy to ameliorate and potentially even *reverse* fibrosis by targeting the progenitor cell response. Other investigators have demonstrated the accumulation of inflammatory monocyte subsets as a key proponent of fibrogenesis and determinant of disease outcomes [6]. Our data presented here indicate that targeting OPN may directly affect the chemokine composition of the periportal environment and thereby alter the accumulation of inflammatory monocytes from the periphery.

The loss of Ly6C^{high} macrophages with OPN neutralization is particularly notable, as is the potential accumulation of Ly6c$^{low/int}$ cells. Furthermore, the chemokines affected by OPN loss such as CCL2 are known to be important effectors of CCR2^{+} macrophage accumulation in CLD. This data implicates OPN as a key regulator of such macrophage accumulation, and indeed to influence the effective composition of the macrophage phenotype. It appears likely that OPN would affect the predominant macrophage population, both directly and indirectly via cholangiocyte chemokine production, towards a phenotype consistent with maintenance of fibrosis. Consistently, neutralization of OPN may effectively skew the macrophage population towards a fibrosis-resolving phenotype. Future investigations are required to

assess the influence of OPN on functionally equivalent subpopulations in humans, such as $CD14^{+}CD16^{+/-}$.

The RNA sequencing data revealed a picture of chemokine gene regulation that is both specific and distinct. In cholangiocytes, the differential genes and pathways affected by OPN were heavily centred on chemokine regulation and inflammatory/immune recruitment. This implies that the functional role of OPN in cholangiocytes may be quite specifically confined to controlling stromal inflammatory interactions. Furthermore, RNA sequencing showed a number of chemokines to be downregulated (also validated by qRT-PCR), rather than just a select few, highlighting the importance of OPN to cholangiocyte expression of this functional grouping. Beyond the in vitro context, it is notable that associations between OPN and chemokine levels were also present in multiple animal models and in MAFLD/MASH patients.

The axis of chemokine ligands and their relevant receptors is increasingly emerging as a clinical target to dampen liver inflammation and the accumulation of fibrosis. The AURORA trial (Phase 3; NCT03028740) investigated a dual-CCR2/CCR5 antagonist (Cenicriviroc) in ameliorating MASH fibrosis [30], demonstrating it was safe and well-tolerated but ultimately failed to show efficacy despite showing promising antifibrotic effect in the earlier CENTAUR phase IIb study. In this context, therapeutic agents targeting OPN may also be worth considering, especially as OPN neutralization demonstrably limits inflammation and fibrosis in animal models [3] but also acts to support chemokine-driven disease progression as reported here. Targeting OPN, either on its own or as an adjuvant therapeutic modality (in addition to chemokine receptor inhibition) may be an attractive proposition.

There is already some evidence from other contexts that implicates OPN in a number of macrophage-related functions [31]. In other tissue types (non-liver), its main role appears to

be the production of chemokines and cytokines, such as CCL2 via activation of NF-κB signalling [32]. In the liver, OPN promotes macrophage infiltration in the carbon tetrachloride chronic injury model, itself acting as a chemoattractant [33], and antibody-mediated neutralization of OPN reduces obesity-induced inflammation and macrophage accumulation in a high fat diet model [34]. Silencing OPN in hepatoma cells reduces their motility and invasiveness, but coculture with highly OPN-expressing macrophages restores motility to normal, highlighting a role for OPN in stromal crosstalk between tumour and macrophages that underlies tumour progression [35]. Although OPN has previously been associated with activation of NF-κB in a range of settings including inflammation and cancer, to our knowledge, the present study is the first report to associate OPN-derived signalling with the *non-canonical* branch.

There are some limitations to this study. OPN is known to be cleaved by matrix metalloproteinases (MMP9, MMP12). How macrophage-secreted MMPs may affect the functional capacity of OPN and what this may imply for OPN-targeting as a therapeutic strategy requires future investigation. In renal fibrosis, for example, MMP9 of both epithelial and macrophage origin may cleave OPN and exacerbate fibrosis progression and further macrophage recruitment [36]. Further work would also be necessary to confirm a causative effect of OPN and associated cholangiocyte chemokine expression in directly mediating the progression from early to late MASH in humans, although this would be challenging to examine interventionally.

In summary, OPN expression in CLD enhances cholangiocyte production of chemokines and promotes accumulation of macrophages, including a proinflammatory monocyte subset. Neutralization of OPN attenuates inflammation-related injury and fibrosis, and is a promising anti-fibrotic strategy.

REFERENCES

1. Pellicoro A, Ramachandran P, Iredale JP, Fallowfield JA. Liver fibrosis and repair: immune regulation of wound healing in a solid organ. *Nat Rev Immunol* 2014;14:181–94.

2. Schuppan D, Kim YO. Evolving therapies for liver fibrosis. *J Clin Invest* 2013;123:1887–901.

3. Coombes JD, Swiderska-Syn M, Dollé L, Reid D, Eksteen B, Claridge L, et al. Osteopontin neutralisation abrogates the liver progenitor cell response and fibrogenesis in mice. *Gut* 2015;64:1120–31.

4. Wang X, Lopategi A, Ge X, Lu Y, Kitamura N, Urtasun R, et al. Osteopontin induces ductular reaction contributing to liver fibrosis. *Gut* 2014;63:1805–18.

5. Syn W-K, Agboola KM, Swiderska M, Michelotti GA, Liaskou E, Pang H, et al. NKT-associated hedgehog and osteopontin drive fibrogenesis in non-alcoholic fatty liver disease. *Gut* 2012;61:1323–9.

6. Tacke F, Zimmermann HW. Macrophage heterogeneity in liver injury and fibrosis. *J Hepatol* 2014;60:1090–6.

7. Ramachandran P, Pellicoro A, Vernon MA, Boulter L, Aucott RL, Ali A, et al. Differential Ly-6C expression identifies the recruited macrophage phenotype, which orchestrates the regression of murine liver fibrosis. *Proc Natl Acad Sci* 2012;109:E3186-3195.

8. Ekstedt M, Franzén LE, Mathiesen UL, Thorelius L, Holmqvist M, Bodemar G, et al. Long-term follow-up of patients with NAFLD and elevated liver enzymes. *Hepatology* 2006;44:865–73.

9. Omenetti A, Syn W-K, Jung Y, Francis H, Porrello A, Witek RP, et al. Repair-related activation of hedgehog signaling promotes cholangiocyte chemokine production. *Hepatology* 2009;50:518–27.

10. Ishimura N, Bronk SF, Gores GJ. Inducible Nitric Oxide Synthase Up-Regulates Notch-1 in Mouse Cholangiocytes: Implications for Carcinogenesis. *Gastroenterology* 2005;128:1354–68.

11. Raschke WC, Baird S, Ralph P, Nakoinz I. Functional macrophage cell lines transformed by abelson leukemia virus. *Cell* 1978;15:261–7.

12. Anders S, Pyl PT, Huber W. HTSeq--a Python framework to work with high-throughput sequencing data. *Bioinformatics* 2015;31:166–9.

13. Love MI, Huber W, Anders S. Moderated estimation of fold change and dispersion for RNA-seq data with DESeq2. *Genome Biol* 2014;15:550.

14. Benjamini Y, Hochberg Y. Controlling the False Discovery Rate: A Practical and Powerful Approach to Multiple Testing. *J R Stat Soc Ser B Methodol* 1995;57:289–300.

15. Eden E, Navon R, Steinfeld I, Lipson D, Yakhini Z. GOrilla: a tool for discovery and visualization of enriched GO terms in ranked gene lists. *BMC Bioinformatics* 2009;10:48.

16. Eden E, Lipson D, Yogev S, Yakhini Z. Discovering motifs in ranked lists of DNA sequences. *PLoS Comput Biol* 2007;3:e39.

17. Huang DW, Sherman BT, Lempicki RA. Bioinformatics enrichment tools: paths toward the comprehensive functional analysis of large gene lists. *Nucleic Acids Res* 2009;37:1–13.

18. Huang DW, Sherman BT, Lempicki RA. Systematic and integrative analysis of large gene lists using DAVID bioinformatics resources. *Nat Protoc* 2009;4:44–57.

19. Supek F, Bošnjak M, Škunca N, Šmuc T. REVIGO summarizes and visualizes long lists of gene ontology terms. *PloS One* 2011;6:e21800.

20. Kanehisa M, Sato Y, Kawashima M, Furumichi M, Tanabe M. KEGG as a reference resource for gene and protein annotation. *Nucleic Acids Res* 2016;44:D457-462.

21. Kanehisa M, Goto S. KEGG: Kyoto encyclopedia of genes and genomes. *Nucleic Acids Res* 2000;28:27–30.

22. Mi Z, Guo H, Russell MB, Liu Y, Sullenger BA, Kuo PC. RNA Aptamer Blockade of Osteopontin Inhibits Growth and Metastasis of MDA-MB231 Breast Cancer Cells. *Mol Ther* 2009;17:153–61.

23. Talbot LJ, Mi Z, Bhattacharya SD, Kim V, Guo H, Kuo PC. Pharmacokinetic characterization of an RNA aptamer against osteopontin and demonstration of in vivo efficacy in reversing growth of human breast cancer cells. *Surgery* 2011;150:224–30.

24. Kleiner DE, Brunt EM, Van Natta M, Behling C, Contos MJ, Cummings OW, et al. Design and validation of a histological scoring system for nonalcoholic fatty liver disease. *Hepatology* 2005;41:1313–21.

25. Moylan CA, Pang H, Dellinger A, Suzuki A, Garrett ME, Guy CD, et al. Hepatic gene expression profiles differentiate presymptomatic patients with mild versus severe nonalcoholic fatty liver disease. *Hepatology* 2014;59:471–82.

26. Coombes JD, Choi SS, Swiderska-Syn M, Manka P, Reid DT, Palma E, et al. Osteopontin is a proximal effector of leptin-mediated non-alcoholic steatohepatitis (NASH) fibrosis. *Biochim Biophys Acta* 2016;1862:135–44.

27. Brunt EM, Kleiner DE, Wilson LA, Unalp A, Behling CE, Lavine JE, et al. Portal chronic inflammation in nonalcoholic fatty liver disease (NAFLD): a histologic marker of advanced NAFLD-Clinicopathologic correlations from the nonalcoholic steatohepatitis clinical research network. *Hepatology* 2009 Mar;49(3):809-20.

28. Richardson MM, Jonsson JR, Powell EE, Brunt EM, Neuschwander-Tetri BA, Bhathal PS, et al. Progressive fibrosis in nonalcoholic steatohepatitis: association with altered regeneration and a ductular reaction. *Gastroenterology* 2007;133:80–90.

29. Gadd VL, Melino M, Roy S, Horsfall L, O'Rourke P, Williams MR, et al. Portal, but not lobular, macrophages express matrix metalloproteinase-9: association with the ductular reaction and fibrosis in chronic hepatitis C. *Liver Int* 2013;33:569–79.

30. Anstee QM, Neuschwander-Tetri BA, Wai-Sun Wong V, Abdelmalek MF, Rodriguez-Araujo G, Landgren H, Park GS, Bedossa P, Alkhouri N, Tacke F, Sanyal AJ. Cenicriviroc Lacked Efficacy to Treat Liver Fibrosis in Nonalcoholic Steatohepatitis: AURORA Phase III Randomized Study. *Clin Gastroenterol Hepatol* 2024 Jan;22(1):124-134.e1.

31. Rittling SR. Osteopontin in macrophage function. *Expert Rev Mol Med* 2011;13:e5.

32. Zheng W, Li R, Pan H, He D, Xu R, Guo TB, et al. Role of osteopontin in induction of monocyte chemoattractant protein 1 and macrophage inflammatory protein 1beta through the NF-kappaB and MAPK pathways in rheumatoid arthritis. *Arthritis Rheum* 2009;60:1957–65.

33. Kawashima R, Mochida S, Matsui A, YouLuTuZ Y, Ishikawa K, Toshima K, et al. Expression of osteopontin in Kupffer cells and hepatic macrophages and Stellate cells in rat liver after carbon tetrachloride intoxication: a possible factor for macrophage migration into hepatic necrotic areas. *Biochem Biophys Res Commun* 1999;256:527–31.

34. Kiefer FW, Zeyda M, Gollinger K, Pfau B, Neuhofer A, Weichhart T, et al. Neutralization of osteopontin inhibits obesity-induced inflammation and insulin resistance. *Diabetes* 2010;59:935–46.

35. Cheng J, Huo D-H, Kuang D-M, Yang J, Zheng L, Zhuang S-M. Human macrophages promote the motility and invasiveness of osteopontin-knockdown tumor cells. *Cancer Res* 2007;67:5141–7.

36. Kui Tan T, Zheng G, Hsu T-T, Ra Lee S, Zhang J, Zhao Y, et al. Matrix metalloproteinase-9 of tubular and macrophage origin contributes to the pathogenesis of renal fibrosis via macrophage recruitment through osteopontin cleavage. *Lab Invest* 2013;93:434–49.

FIGURE LEGENDS

Figure 1. A) Cholangiocyte (603B) coexpression of keratin 19 and OPN, relative to RPS9 housekeeping. qPCR product on agarose gel. B) Secretion of OPN by 603B detected by ELISA of conditioned media. *p<0.05. C) Western blot showing short-hairpin knockdown of OPN. D) qRT-PCR detection of chemokines CCL2, CXCL1 and CCL5 with OPN knockdown. E) Cytometric bead array detection of chemokines secreted in 603B conditioned media. *p<0.05 shOPN vs shScr; unpaired t-test with Welch correction.

Figure 2. A) NF-κB activity detected by TransAM® DNA-binding ELISA of family subunits. Lysates from shScr and shOPN 603B cholangiocytes are compared to quantify transcription factor activation and the specific NF-κB subunit. Activity (a.u. Mean±SD) shown, shOPN vs shScr unpaired t-test with Welch correction. B) Western blot visualizing equivalent total protein levels of p65 and α-actinin used as loading control.

Figure 3. Macrophage activity. Transmigration assays: RAW264.7 macrophages exposed to conditioned media from 603B cholangiocytes. Number of migrated cells shown. Conditioned media was treated with several schemes: A) control IgG, OPN-neutralizing antibody, chemokine-neutralizing antibodies (against CCL2/MCP1, CXCL1/KC and CCL5/RANTES) and recombinant OPN; B) sham aptamer, OPN-neutralizing aptamer and recombinant OPN; C) conditioned media from shScr and shOPN 603B cholangiocytes. D) Macrophage expression of activation markers Class II MHC Transactivator (Ciita) and Arginase 1 (Arg1) after treatment with conditioned media from shScr or shOPN 603B cholangiocytes. qRT-PCR data shown, Mean±SD, p<0.05, shOPN vs shScr, unpaired t-test with Welch correction.

Figure 4. Murine liver injury models treated with OPN-neutralizing aptamer. A) Liver injury (ALT) and fibrogenesis markers (αSMA and Col1a1). *p<0.05. B) Sirius red histology for fibrosis *p<0.05, unpaired t-test with Welch correction. C) Chemokine mRNA levels by qRT-PCR analysis whole liver tissue from MCD-model and CCl4-model mice. *p<0.05 vs Normal, **p<0.05 vs Sham aptamer+MCD, unpaired t-test with Welch correction.

Figure 5. Accumulation of inflammatory monocytes in murine liver injury. MCD model shown. A) Immunohistochemical detection of macrophages labelled by the F4/80 marker with brown chromogen. B) Flow cytometric analysis of inflammatory monocyte subsets from total liver, gated on $CD11b^{+}F4/80^{+}$. The Ly-6C antigen was used to distinguish 'pro-fibrogenic' $Ly\text{-}6C^{High}$ monocytes and 'restorative' $Ly\text{-}6C^{Low}$ monocytes. *p<0.05 vs sham, unpaired t-test with Welch correction.

Figure 6. Human MASH. A) Inflammatory monocyte accumulation detected by CD68 immunohistochemistry of MASH versus normal liver. B) Progression from early to advanced MASH is accompanied by increased OPN and chemokines IL-8 and CCL2. Microarray data shown. P<0.05 Advanced MASH vs Early MASH. C) Dual immunohistochemistry with cholangiocyte marker CK19 (green) and OPN (brown) in normal liver and MASH. Quantification of double positive cells is shown, including the proportion of $CK19^{+}$ cells that are also OPN^{+}. Mean±SD; *p<0.05, unpaired t-test with Welch correction.

Title Pages

Osteopontin promotes cholangiocyte secretion of chemokines to support macrophage recruitment and fibrosis in MASH.

Authors:

Jason D. Coombes[1,2,14], Paul P Manka[1,2,3], Marzena Swiderska-Syn[13], Danielle T Vannan[5,6], Antonio Riva[2,7], Lee C Claridge[8], Cynthia Moylan[4], Ayako Suzuki[4], Marco A Briones-Orta[1,2], Rasha Younis[1], Naoto Kitamura[1], Svenja Sydor[3], Shanna Bittencourt[10], Zhiyong Mi[9], Paul C. Kuo[9], Anna Mae Diehl[4], Leo A van Grunsven[10], Shilpa Chokshi[2,7], Ali Canbay[3], Manal F. Abdelmalek[11], Patricia Aspichueta[12], Salvatore Papa[13], Bertus Eksteen[5,6], Wing-Kin Syn[1,12,14]

[1] Regeneration and Repair, Institute of Hepatology, Foundation for Liver Research, London, United Kingdom.

[2] Faculty of Life Sciences and Medicine, King's College London, London, United Kingdom.

[3] Gastroenterology and Hepatology, University Clinic Bochum, Bochum, Germany.

[4] Division of Gastroenterology, Department of Medicine, Duke University, Durham, North Carolina.

[5] Snyder Institute for Chronic Diseases, University of Calgary, Alberta, Canada.

[6] Aspen Woods Clinic, Calgary, Alberta, Canada

[7] Viral Hepatitis and Alcohol Research Group, Institute of Hepatology, Foundation for Liver Research, London, United Kingdom.

[8] Department of Hepatology, Leeds Teaching Hospital NHS Trust, UK.

[9] Department of Surgery, University of South Florida, Tampa, Florida.

[10] Liver Cell Biology, Vrije Universiteit, Brussels, Belgium.

[11] Division of Gastroenterology and Hepatology, Mayo Clinic, Rochester, Minnesota.

[12] Department of Physiology, Faculty of Medicine and Nursing, University of the Basque Country, EPV/EHU, Leioa.

[13] Leeds Institute of Medical Research, St. James's University Hospital, University of Leeds, Leeds, UK.

[14] Division of Gastroenterology and Hepatology, School of Medicine, Saint Louis University, Saint Louis, Missouri, USA.

Corresponding Author: Wing-Kin Syn, MD PhD, Division of Gastroenterology and Hepatology, Saint Louis University School of Medicine. wingkin.syn@health.slu.edu

Financial Support:

This study was funded predominantly by CORE-UK (WKS), BRET (WKS), EASL (WKS, PPM), The Foundation for Liver Research London (WKS, SC), the University of Birmingham (WKS), and GASL (PPM). Additional funding was provided by the National Institute of Health R01 DK077794 (AMD), Belgian Federal Science Policy Office (Interuniversity Attraction Poles program - P6/20 and P7/83-HEPRO) (LvG), the Brussels Capital Region (INNOVIRIS Impulse programme-Life Sciences 2007 and 2011; BruStem) (LvG), the Institute for the Promotion of Innovation through Science and Technology in Flanders (SBO-IWT-090066 HEPSTEM) (LvG), the Natural Sciences and Engineering Research Council of Canada Postgraduate Doctoral Scholarship (BE), the Alberta Innovates Technology Futures Graduate Scholarship (BE), DFG (German Research Association) CA267/8-1 (AC), and the Wilhelm Lapitz Foundation (AC).

Disclosures: None declared.

Abbreviations:

CLD, Chronic liver disease

CCL, Chemokine (C-C motif) ligand

CCR, CC chemokine receptors

CD, Cluster of differentiation

CXCL, Chemokine (C-X-C motif) ligand

HSC, Hepatic stellate cell

LPC, Liver progenitor cell

Ly6c, Lymphocyte antigen 6 complex

MAFLD, metabolic dysfunction-associated fatty liver disease

MASH, metabolic dysfunction-associated alcoholic steatohepatitis

OPN, Osteopontin

Acknowledgements:

Dr. G. J. Gores (Mayo Clinic, Rochester, MN) and Yoshiyuki Ueno (Tohoku University, Sendai, Japan) for providing the murine immature ductular cell line (603B). Karine Vanacker and Frederic Flamant (IGSL, Lyon), Benjamin Gillet and Sandrine Hughes (PSI, IGSL) for supplying materials and assistance with RNA sequencing.

ABSTRACT

Background and aims

Osteopontin (OPN) promotes the ductular reaction and is a major driver of chronic liver disease (CLD) progression. Although CLD is characterized by the accumulation of inflammatory cells including macrophages around the peri-portal regions, the influence of OPN on recruitment is unclear. We investigated the role of OPN in cholangiocyte chemokine production and macrophage recruitment by combining *in vivo*, *in vitro*, and *in silico* approaches.

Methods

The effects of OPN on cholangiocyte chemokine production and macrophage migration were assessed in culture, alongside RNA-sequencing to identify genes and pathways affected by OPN depletion. Murine liver injury models were used to assess liver chemokine expression and liver macrophage/monocyte recruitment. OPN and chemokine expression were analysed in liver tissue and plasma from biopsy-proven MASH patients.

Results

OPN-knockdown in cholangiocytes reduced chemokine secretion. RNA-sequencing showed OPN-related effects clustered around immunity, chemotaxis and chemokine production. Macrophage exposure to cholangiocyte-conditioned media showed OPN supported migration via chemokines CCL2, CCL5 and CXCL1. These effects were related to NF-κB signalling. Murine liver fibrosis was accompanied by upregulated liver OPN, CCL2, CCL5, and CXCL1 mRNA, and accumulation of liver CD11b/F4/80^{+}CCR2^{high} macrophages but treatment with OPN-specific neutralizing aptamers reduced fibrosis, chemokine mRNAs and accumulation of liver CD11b/F4/80^{+}CCR2^{high}/ Ly6C^{high} inflammatory monocytes. In human MASH, liver OPN correlated with chemokines CCL2 and IL8 in association with portal injury and fibrosis. Plasma OPN, serum CCL2 and IL8 also increased with fibrosis stage.

Conclusions

OPN promotes cholangiocyte chemokine secretion and the accumulation of pro-inflammatory monocytes. These data support neutralization of OPN as an anti-inflammatory and anti-fibrotic strategy.

[249 words]

Keywords

Osteopontin, Chemokine, Cholangiocyte, Macrophage, MASH, Fibrosis.

INTRODUCTION

Despite considerable progress towards understanding the cellular and inflammatory factors that drive chronic liver disease (CLD) progression, specific therapies that ameliorate CLD still elude clinical translation. Targeting liver fibrosis, the most predictive indicator of disease progression and negative prognosis would present attractive modalities for therapeutic intervention [1,2].

We have reported that Osteopontin (OPN) is a key driver of liver fibrogenesis via activation of hepatic stellate cells (HSCs) and progenitor cells [3]. OPN mediates crosstalk between periportal and stromal cells and drives the ductular reaction which is highly linked to fibrogenesis [3,4]. An acidic member of the small integrin-binding ligand N-linked glycoprotein (SIBLING) family of proteins, OPN is abundantly expressed in a wide range of tissues during inflammation and repair. It is secreted by various cell-types including epithelial cells, T cells, dendritic cells and macrophages, and its expression is induced by oxidative stress, growth factors (e.g. PDGF, TGFβ), and cytokines (e.g. IL6, TNFα). In normal liver, OPN is expressed by cholangiocytes, HSCs, progenitors, and immune cells (macrophages, DCs, B and T cell subsets). To date, OPN has been shown to be upregulated in human CLD (viral hepatitis B and C, NAFLD/MAFLD, ALD, PBC, PSC, autoimmune hepatitis) and in models of liver injury (bile-duct ligation, biliary fibrosis; methionine-choline deficient diet (MCD), MASH-fibrosis; carbon tetrachloride injection (CCl_4), fibrosis). Liver and serum/plasma OPN levels correlate with severity of liver fibrosis in humans and mice [5].

A specific role for OPN in macrophage activation and recruitment in CLD, however, remains unclear. In liver, inflammatory monocytes, particularly myeloid-derived macrophages, influence pro-inflammatory and pro-fibrotic progression and through crosstalk maintain HSC activation [6]. Interestingly, depending on macrophage *subset* as defined by activation

markers, there also appears to be a key role in resolving fibroinflammatory disease in murine CLD models [7]. CD11b^{high}F4/80^{int}Ly6C^{high} infiltrating monocyte-derived macrophages accumulate early in disease to promote fibrosis whereas CD11b^{high} F4/80^{int}Ly6C$^{int//low}$ macrophages regulate fibrosis resolution by the expression of more MMPs.

As the nature of the inflammatory response appears to influence the course and outcome of CLD, directing therapy at the recruitment of subsets and/or signals involved could attenuate liver injury and fibrosis. Furthermore, portal fibrosis has been shown to be the best predictor of liver complications during follow-up [8]. Previous work has indicated that inflammatory cell accumulation in portal tracts is influenced by activated-HSC derived Hedgehog (Hh) ligands, which induce cholangiocytes to secrete chemokines including CXCL16 and thereby recruit inflammatory NKT cells [9]. Hh signals drive OPN production and this mechanism of inflammatory recruitment is shown to drive fibrogenesis [5]. Additionally, we have reported that the greatest levels of OPN expression in the injured liver are in the periportal regions, and in colocation with the cholangiocyte marker Keratin 19 [3]. We therefore sought to investigate whether OPN modulates cholangiocyte chemokine secretion that leads to macrophage recruitment.

We have combined multiple investigatory disciplines, including human data, multiple animal models, cell culture and bioinformatic analysis of next-generation gene sequencing. We find that OPN critically affects cholangiocyte chemokine secretion to promote macrophage recruitment in CLD and moreover may promote an inflammatory response that favours fibrosis progression.

EXPERIMENTAL PROCEDURES

Cellular analyses

The murine cholangiocyte cell line 603B and murine macrophage line RAW264.7 were maintained according to standard protocols [10,11]. For migration experiments, 603B-conditioned media was transferred to the bottom chamber of a standard transwell apparatus (Nunc, ThermoFisher, Paisley, UK); RAW264.7 were seeded into the top chamber on a polycarbonate membrane with 8 um pores. Migrated cells were counted using coomassie blue staining of cells translocated to the underside of the membrane, using at least 15 nonoverlapping fields from two independent experiments.

Stable OPN knockdown using short-hairpin RNA was achieved as described [3]. OPN knockdown 603B cells (shOPN-603B) were compared with non-targeting scrambled shRNA (shScr-603B). For select experiments, conditioned media was treated with either OPN-neutralizing aptamer ("OPN Apt", versus sham control aptamer "Sham Apt"), recombinant OPN (rOPN, 100 ng/mL, R&D), OPN-neutralizing antibody (2 ug/ mL R&D) neutralizing antibodies against CCL2, CXCL1, CCL5 or control IgG (3 µg/mL; 0.5 ug/uL; 0.5 ug/uL and 3 ug/mL, respectively).

Molecular RNA Sequencing and bioinformatics analyses

RNA was collected from snap-frozen 603B cell pellets ($2x10^6$ cells) using a standard Trizol protocol. RNA sequencing was performed on an Ion Proton™ (Life Technologies) Next Generation Sequencing platform (at the Institut de Génomique Fonctionnelle, Lyon, France). The Htseq software [12] count feature (Reserve strand setting) was used to map reads (Bam files) on UCSC mouse genome release Mm10 and generate count tables. The Deseq2 R package from Bioconductor was used to analyze each count table separately [13]. Only genes

exceeding a conservative threshold of at least 10 reads in one sample were kept (considered to be expressed; False discovery rate 0.05). Selected genes were considered "Called Differential" if they satisfied a Benjamini-Hochsberg [14] p-adjusted value <0.05 and had Log2-fold change either >1 or <-1. Gene ontologies and functional enrichment were analysed using two modalities: GOrilla [15,16] and DAVID [17,18] software. Multiple GO terms were synthesized in ReviGO to simplify functional categories and reduce redundancy [19]. Specific altered pathways detected from RNA-Seq data were generated from the KEGG database [20,21].

Animal models

Mice were housed in 12-hr light/dark cycle with food and water ad libitum. Liver samples for RNA analyses and immunohistochemistry were taken at the indicated timepoints. Animal handling was conducted in line with the US National Research Council's Guide for the Care and Use of Laboratory Animals, the US Public Health Service's Policy on Humane Care and Use of Laboratory Animals, the UK Animals (Scientific Procedures) Act 1986 Amendment Regulations (SI 2012/3039), and European Union Directive 2010/63/EU with approval by the relevant institutional committees of Duke University; Vrije Universiteit Brussel, Belgium; University of Calgary, Canada.

Murine Methionine-choline deficient diet (MCD), 3,5,-Diethoxycarbonyl-1,4-dihydrocollidine diet (DDC) and Carbon tetrachloride (CCl_4) models were performed as described [3]. MCD mice (n=5/group) were fed methionine-choline deficient (MCD) diet or control chow for 5 weeks to induce metabolic dysfunction-associated steatohepatitis (MASH) fibrosis. CCl_4 mice (n=5/group) received twice-weekly intraperitoneal injections of CCl_4 (0.5

mg/kg, Sigma-Aldrich) or vehicle (mineral oil) for 6 weeks. DDC mice (n=5/group) were fed the dihydrocollidine (DDC) diet for 3 weeks to induce biliary-type fibrosis.

OPN neutralization

Mice received OPN-specific aptamers (specifically neutralize circulating-extracellular OPN) or sham-aptamers (negative control) [22,23] by tail-vein injections in the final week of dietary or chemical challenge (n=10/study; 5/group; four injections (alternate days) total per mouse; 200 µg in 100 µL of PBS). Mice were sacrificed 24 h after the final aptamer dose.

Histology and Immunohistochemistry

Liver tissue was formalin-fixed, paraffin-embedded, and cut into 5-µm sections. To quantify liver fibrosis, five-micron sections were stained with picrosirius red (Sigma, St. Louis, MO) and counterstained with fast green (Sigma, St. Louis, MO). Immunohistochemical staining was performed as previously described [3] to detect OPN, αSMA, F4/80, CD68 and Cytokeratin 19 (CK19) using procedures described in ***Supplemental Methods***.

Human Histology and tissue analyses

Studies using human material from Duke University Hospital were conducted in accordance with NIH and Institutional guidelines for human subject research and the Declaration of Helsinki (2008). For formalin-fixed, paraffin-embedded (FFPE) sections, deidentified samples were obtained from explanted liver tissue from individuals undergoing transplantation for MASH-cirrhosis, and normal tissues were obtained from excess split-liver grafts. Total liver RNA was obtained from freshly explanted and snap-frozen MASH.

Biobanked samples (Duke NAFLD/MAFLD repository) were collected on same day as acquired liver histology.

Tissue Microarray and Luminex cytokine profile

Transcriptomic data was generated from frozen liver biopsy tissue obtained from patients previously enrolled in the Duke University Health System NAFLD/MAFLD Biorepository. Clinically-indicated liver biopsies and liver histology were graded and scored for MAFLD-related injury and fibrosis according to published criteria [24]. Transcriptomic data from 72 patients was analysed, including 40 with mild MAFLD, defined as fibrosis stages 0 or 1, and 32 with severe MAFLD, defined as fibrosis stages 3 or 4. The biorepository, patient demographics, RNA preparation and generation of genomic data have been described previously [25]. Briefly, microarray hybridization was performed using Affymetrix Human Genome U133 Plus 2.0 GeneChip arrays (Affymetrix, Santa Clara, CA). Differential gene expression for *CXCL8*, *CCL2* and *SPP1* was determined using two sample Student's t-test assuming equal variances (Matlab, Mathworks, Natick, MA). Cytokine profiling was performed on biobanked serum and plasma samples (123 patients) using a Luminex analyte panel according to manufacturer's instructions (and **Supplemental methods**).

Protein detection and gene expression

Semiquantitative real-time PCR (qRT-PCR), western blotting and agarose gel electrophoresis were performed as described in **Supplemental methods.** NF-κB activity and specific subunit was detected using TransAM® NFκB p50, p52, p65 & Family Kits (Active Motif, Carlsbad, CA). Chemokines secreted in culture were measured by cytometric bead array (BD

Biosciences, Oxford, UK). ELISA detection of secreted OPN in media was performed as per kit manufacturer instructions (R&D Systems, Abingdon, UK).

Statistical analyses

For groupwise comparisons, analyses were performed using Graph-Pad Prism 4 software (GraphPad Software, La Jolla, CA) and data presented as mean±SEM. For two independent groups unpaired t-test was used with Welch correction to tolerate unequal variances, and for multiple comparisons a one-way ANOVA with Tukey's MCT post-hoc correction. Statistically significant differences were considered at $p \leq 0.05$.

RESULTS

Osteopontin is associated with chemokine production by cholangiocytes

The role of OPN in cholangiocyte chemokine secretion was investigated in vitro using the 603B cell line, which highly expresses both OPN and the cholangiocyte/ductular marker keratin 19 (**Figure 1A**) and secretes a copious amount of OPN as detected by ELISA of conditioned media (**Figure 1B**). Knockdown of OPN using lentivirus-mediated short-hairpin RNA targeting Osteopontin (shOPN) achieved approximately 65% knockdown versus non-targeting scrambled control (shScr) (**Figure 1C**) (Western quantitation shown in **Supplemental Figure 7**). We initially examined *production* of selected chemokines CCL2 (MCP-1), CXCL1 (KC/FSP/Gro1) and CCL5 (RANTES) and found that knockdown of OPN was associated with significantly downregulated mRNA of these chemokines (80%, 40% and 95% downregulation, respectively) (**Figure 1D**). Similar reductions were found for *secretion* of these chemokines, as detected by cytometric bead array examination of 603B conditioned media (approx. 75%, 60% and 85% loss of secretion, respectively) (**Figure 1E**).

To gain a wider appreciation of all the chemokines that may be affected and to investigate the wide array of signalling processes that could affect chemokine production in relation to OPN, we applied Next Generation RNA Sequencing (RNAseq). Appreciable levels of transcript were detected in 11,728 genes. Among these, we determined 670 genes to be significantly altered (Benjamini-Hochsberg p_{adj} <0.05), of which 192 genes were altered by more than 1x log_2Fold, a conservative cutoff which may underline functionally significant downregulation. Among these significantly altered genes, many of the most highly altered were chemokines (listed in **Table 1**). We detected alterations in 17 chemokines, of which 14/17 were downregulated, 10 by more than 1xlog_2fold and with statistical significance. In addition to aforementioned CCL2, CXCL1 and CCL5, significantly downregulated chemokines included

CXCL16, CXCL11, CXCL10, CCL9, CCL7, CX3CL1 (Fractalkine) and CXCL5. To account for the possibility of error associated with the high-throughput RNAseq process we independently verified these chemokines using qRT-PCR, which showed similarly consistent levels (***Supplemental Figure 1***), indicating the accuracy of the RNAseq and the robustness of chemokine downregulation.

The functional significance of the full range of altered genes detected by RNAseq was interrogated using Gene Ontology (GO) analysis to identify the most strongly-represented functional clusters among the differentially expressed genes. Two different modalities, GOrilla software and DAVID software, provided remarkably similar results (**Supplemental Table 3**). The enriched terms heavily favoured *chemokine and immune cell recruitment functional terms*, especially among the most significant hits, implying a role for OPN in these processes. The predominance of these terms also supports the primacy of these functions in relation to OPN i.e., the main function of OPN in cholangiocytes appears to be highly related to chemokine production and signals for chemotaxis/immune recruitment. A synthesis of all GO terms reported by GOrilla using ReviGO software to sort functional groupings also demonstrates that overwhelmingly the largest effect of OPN was on immune/inflammatory recruitment and chemokine/cytokine production (***Supplemental Figure 2***). Additionally, interrogation of altered genes via the KEGG signalling database indicated a robust role for OPN in chemokine/cytokine production and immune recruitment signalling pathways, which were the predominantly represented pathways (**Supplemental Table 4**).

OPN promotes non-canonical NF-κB signalling in cholangiocytes

Some affected GO terms were related to NF-κB signalling, which is known to be one of the main pathways for chemokine production and is also associated with activation by OPN. We

therefore investigated whether OPN was driving NF-κB activity in cholangiocytes. NF-κB activity assays showed that loss of OPN in 603B was associated with suppression of the *non-canonical* NF-κB pathway (repression of p52 and RelB activity in shOPN relative to shNS), but not the canonical branch (there was no suppression of p50, c-Rel, or p65 activity) (**Figure 2**). This implies that OPN stimulates a non-canonical NF-κB signalling mechanism in cholangiocytes. Searching the RNAseq data for known NF-κB-responsive *target* genes, aside from the chemokines identified already, indicates 25 target genes were significantly altered in shOPN cholangiocytes (Benjamini-Hochsberg p_{adj} <0.05); 24 out of these 25 genes were *downregulated* and 12 out of these 25 by more than 1 log_2fold (***Supplemental Table 5***). Three NF-κB-family genes were also downregulated: *Nfkbid* ($IκB_{NS}$, atypical IκB protein, modulator of nuclear NF-κB function), *Nfkbia* (IκBα, canonical inhibitor of NF-κB) and *Nfkb2* (NF-κB p100 subunit).

OPN enhances cholangiocyte-associated macrophage migration

To explore whether this deficiency in chemokine production affected macrophage recruitment we treated RAW264.7 macrophages with conditioned media from 603B cholangiocytes. 603B-conditioned media stimulated macrophage migration across transwell membranes (**Figure 3A**), however macrophage migration was comparably reduced with conditioned media from shOPN cholangiocytes (**Figure 3C**). Furthermore, neutralizing the chemokines CCL2, CXCL1 and CCL5 (using neutralizing antibodies; **Figure 3A**) abrogated transmigration in comparison to wildtype cholangiocyte conditioned media treated with non-specific IgG-control. Neutralization of OPN by antibody or by aptamer similarly reduced macrophage transmigration, whereas spiking the conditioned media with recombinant OPN (rOPN) enhanced migration (**Figures 3A, 3B**). These results indicate that OPN can directly

enhance cholangiocyte-stimulated macrophage migration, but also *indirectly* instruct the recruitment capacity of cholangiocytes by influencing the chemokine composition of the cholangiocyte secretome. The activation phenotype of macrophages also appears to be affected, as knockdown of OPN in 603B was associated with decreased expression of the inflammatory activation marker CIITA and increased expression of the immunomodulatory/resolving activation marker Arg1 (**Figure 3D**).

OPN neutralization inhibits inflammatory monocyte accumulation and chemokine expression in mouse models of liver injury.

To investigate whether the influence of OPN on inflammatory monocyte accumulation extends to the *in vivo* context we studied murine models of liver injury and fibrosis. We used an interventional approach, whereby circulating OPN was targeted by specific neutralizing-aptamer treatment in the MCD dietary model and the CCl_4 toxicity model. Additionally, biliary-type fibrosis was modelled using the DDC diet. We have previously shown the aptamer neutralization modality to be effective in these murine models and comparable to a neutralizing antibody modality [3].

MCD model. Consistent with our previous reports [3,26], in a 5-week MCD model, mice treated with Osteopontin-neutralizing aptamer had approximately 50% reductions in ALT, which would be in line with reduced inflammation. Simultaneously, fibrogenesis and HSC activation was also ameliorated (whole liver tissue *aSMA* mRNA by 2.1-fold; *Col1a1* mRNA by 2.2-fold; **Figure 4A**). Sirius red histology also demonstrated markedly reduced fibrosis with OPN neutralization (**Figure 4B**). Moreover, consistent with the *in vitro* findings, the induction of chemokines CCL2, CXCL1 and CCL5 was significantly ameliorated by OPN neutralization (whole liver tissue mRNA; **Figure 4C**).

CCl_4 model. Similar results were present in the 6-week CCl_4 model. The reductions in fibrogenesis (*aSMA* and *Col1a1)*, as we have previously reported with OPN-neutralizing aptamer treatment in the CCl_4 model [3], and reductions in collagen-rich fibrotic matrix were accompanied by significant reductions in chemokine mRNA, whereby the induction of CCL2, CXCL1 and CCL5 was almost completely reversed by OPN neutralization (**Figure 4C**).

DDC model. As a model of biliary-type fibrosis, we used a 3-week DDC model with 1.5 weeks OPN aptamer treatment. Consistent with the MCD and CCl_4 models, OPN neutralization was associated with significantly reduced levels of chemokines CCL2, CXCL1 and CCL5 (whole tissue mRNA; ***Supplemental Figure 4***).

Inflammatory cell recruitment. The presence of inflammatory cell recruitment was assessed using immunohistochemical detection of the F4/80 marker. Chronic liver injury is typically associated with accumulation of F4/80-positive cells, particularly around periportal regions (**Figure 5A**). In the MCD model, this accumulation was significantly reduced in mice treated with OPN neutralization. Flow cytometry of homogenized whole liver tissue was also used to detect inflammatory monocytes. In a supplemental study using a neutralizing antibody modality, OPN neutralization resulted in a 23% reduction in the accumulation of $CD11b^{high}F4/80^{high}$ inflammatory monocytes (***Supplemental Figure 5***).

Due to marked heterogeneity among inflammatory monocyte subsets, we sought to functionally characterize differences in accumulation influenced by OPN. In other murine studies, it has been shown that $CD11b^{high}F4/80^{int}Ly6C^{high}$ infiltrating monocyte-derived macrophages accumulate early in disease to promote fibrosis whereas $CD11b^{high}F4/80^{int}Ly6C^{int/low}$ macrophages regulate fibrosis resolution by expressing more

MMPs [7]. Notably, we find that OPN neutralization is also associated with reduced accumulation of the CD11b^{high}F4/80^{int}Ly6C^{high} subset (5.3% vs 1.6% of cells gated on CD11b^{+}F4/80^{+}) associated with inflammation and maintenance of fibrosis. Additionally, the CD11b^{high}F4/80^{int}Ly6C$^{int/low}$ population (associated with fibrosis resolution) was increased with OPN neutralization (**Figure 5B**). Altogether, these combined data indicate that *OPN supports inflammatory monocyte recruitment, particularly a profibrotic subset*. Furthermore, these data are consistent with OPN neutralization as a modality to suppress the pro-inflammatory monocyte activity that maintains fibrosis.

OPN and chemokine expression is associated with portal injury and fibrosis in human MASH

Immunohistochemical detection of the macrophage marker CD68 indicates a marked accumulation in MASH patients compared with normal liver (**Figure 6A**). This was particularly evident in portal regions, in close proximity to cholangiocytes. Dual-immunohistochemistry was performed to observe co-localisation of OPN with cholangiocytes (CK19 marker). There was a very apparent colocalization of CK19 and OPN (**Figure 6C**). with a high degree of cellular coexpression. Coexpression increased significantly in MASH vs normal liver, consistent with a regulatory role of OPN.

Portal inflammation and portal fibrosis have been shown to have consistent histological association with advanced MAFLD [27]. Our analysis of a luminex cytokine profile of 123 histologically evaluated MAFLD patients indicated significant associations with histological features of MASH. Specifically, between serum OPN and both *portal inflammation* and *portal fibrosis* (p=0.0006, positive; p=0.0008, positive; Spearman Rho.), Additionally, chemokines CCL2 and IL-8 (human functional equivalent of murine CXCL1/KC) also

positively correlated with both *portal inflammation* (p=0.0012 and p=0.038, respectively) and *portal fibrosis* (p=0.0025 and p=0.0001, respectively) (**Supplemental Table 6**).

In a separate analysis, OPN and chemokine expression was further explored in the context of fibrosis severity. Transcriptomic data was generated from biopsies of MASH histologically-proven and staged patients (*n*=72; 40 mild MAFLD, defined as fibrosis stage 0 or 1; 32 severe MAFLD, defined as fibrosis stage 3 or 4) using Affymetrix Human Genome U133 Plus 2.0 GeneChip microarrays. Chemokines CCL2 and IL8 were upregulated (approximately 50% and 140%, respectively) in livers with *advanced* MASH (i.e. *advanced fibrosis*) vs. *early* MASH (i.e. *early fibrosis*), while OPN was similarly increased from early to advanced MASH (approximately 175%) (**Figure 6B**).

DISCUSSION

We report that OPN drives chemokine production in cholangiocytes, which serves to recruit inflammatory monocytes / macrophages in chronic liver injury. Loss of OPN was associated with markedly reduced expression and secretion of a range of chemokines including CCL2, CXCL1 and CCL5 among others. This was associated with OPN-related stimulation of NF-κB signalling. Of novel importance, this was not via the canonical branch of the pathway, but via non-canonical NF-κB involvement. Additionally, OPN enhances cholangiocyte associated macrophage migration by both indirect and direct effects. Moreover, in murine models of chronic injury, OPN *neutralization* was associated with reduced accumulation of inflammatory monocytes (F4/80^{+}). The presence of OPN supported the recruitment of *profibrogenic* subpopulations (murine Ly6C^{high}), whereas OPN neutralization was associated with loss of chemokine secretion and the relative accumulation of a fibrosis resolution-associated subpopulation (Ly6C^{low}). Together, these data suggest that, in the liver, OPN is a

key driver of inflammatory macrophage recruitment via modulation of cholangiocyte chemokine expression and non-canonical NF-κB signalling.

The association of OPN with portal inflammation and fibrosis in human MASH, and indeed with worsening MASH is consistent with previous observations that OPN drives the ductular response [3] and is a regulator of immune recruitment [5] to facilitate fibrosis. The ductular reaction is recognised as a key determinant of progressive fibrosis in patients with MASH [28]. Furthermore, portal macrophage activity is specifically associated with the ductular reaction and fibrosis progression in CLD [29]. Targeting a molecular determinant of portal macrophage recruitment, especially one that promotes fibrosis, would be a critical avenue to intervene in fibrosis progression and halt worsening MASH. We have previously demonstrated that OPN neutralization is a viable strategy to ameliorate and potentially even *reverse* fibrosis by targeting the progenitor cell response. Other investigators have demonstrated the accumulation of inflammatory monocyte subsets as a key proponent of fibrogenesis and determinant of disease outcomes [6]. Our data presented here indicate that targeting OPN may directly affect the chemokine composition of the periportal environment and thereby alter the accumulation of inflammatory monocytes from the periphery.

The loss of Ly6C^{high} macrophages with OPN neutralization is particularly notable, as is the potential accumulation of Ly6c$^{low/int}$ cells. Furthermore, the chemokines affected by OPN loss such as CCL2 are known to be important effectors of CCR2^{+} macrophage accumulation in CLD. This data implicates OPN as a key regulator of such macrophage accumulation, and indeed to influence the effective composition of the macrophage phenotype. It appears likely that OPN would affect the predominant macrophage population, both directly and indirectly via cholangiocyte chemokine production, towards a phenotype consistent with maintenance of fibrosis. Consistently, neutralization of OPN may effectively skew the macrophage population towards a fibrosis-resolving phenotype. Future investigations are required to

assess the influence of OPN on functionally equivalent subpopulations in humans, such as $CD14^{+}CD16^{+/-}$.

The RNA sequencing data revealed a picture of chemokine gene regulation that is both specific and distinct. In cholangiocytes, the differential genes and pathways affected by OPN were heavily centred on chemokine regulation and inflammatory/immune recruitment. This implies that the functional role of OPN in cholangiocytes may be quite specifically confined to controlling stromal inflammatory interactions. Furthermore, RNA sequencing showed a number of chemokines to be downregulated (also validated by qRT-PCR), rather than just a select few, highlighting the importance of OPN to cholangiocyte expression of this functional grouping. Beyond the in vitro context, it is notable that associations between OPN and chemokine levels were also present in multiple animal models and in MAFLD/MASH patients.

The axis of chemokine ligands and their relevant receptors is increasingly emerging as a clinical target to dampen liver inflammation and the accumulation of fibrosis. The AURORA trial (Phase 3; NCT03028740) investigated a dual-CCR2/CCR5 antagonist (Cenicriviroc) in ameliorating MASH fibrosis [30], demonstrating it was safe and well-tolerated but ultimately failed to show efficacy despite showing promising antifibrotic effect in the earlier CENTAUR phase IIb study. In this context, therapeutic agents targeting OPN may also be worth considering, especially as OPN neutralization demonstrably limits inflammation and fibrosis in animal models [3] but also acts to support chemokine-driven disease progression as reported here. Targeting OPN, either on its own or as an adjuvant therapeutic modality (in addition to chemokine receptor inhibition) may be an attractive proposition.

There is already some evidence from other contexts that implicates OPN in a number of macrophage-related functions [31]. In other tissue types (non-liver), its main role appears to

be the production of chemokines and cytokines, such as CCL2 via activation of NF-κB signalling [32]. In the liver, OPN promotes macrophage infiltration in the carbon tetrachloride chronic injury model, itself acting as a chemoattractant [33], and antibody-mediated neutralization of OPN reduces obesity-induced inflammation and macrophage accumulation in a high fat diet model [34]. Silencing OPN in hepatoma cells reduces their motility and invasiveness, but coculture with highly OPN-expressing macrophages restores motility to normal, highlighting a role for OPN in stromal crosstalk between tumour and macrophages that underlies tumour progression [35]. Although OPN has previously been associated with activation of NF-κB in a range of settings including inflammation and cancer, to our knowledge, the present study is the first report to associate OPN-derived signalling with the *non-canonical* branch.

There are some limitations to this study. OPN is known to be cleaved by matrix metalloproteinases (MMP9, MMP12). How macrophage-secreted MMPs may affect the functional capacity of OPN and what this may imply for OPN-targeting as a therapeutic strategy requires future investigation. In renal fibrosis, for example, MMP9 of both epithelial and macrophage origin may cleave OPN and exacerbate fibrosis progression and further macrophage recruitment [36]. Further work would also be necessary to confirm a causative effect of OPN and associated cholangiocyte chemokine expression in directly mediating the progression from early to late MASH in humans, although this would be challenging to examine interventionally.

In summary, OPN expression in CLD enhances cholangiocyte production of chemokines and promotes accumulation of macrophages, including a proinflammatory monocyte subset. Neutralization of OPN attenuates inflammation-related injury and fibrosis, and is a promising anti-fibrotic strategy.

REFERENCES

1. Pellicoro A, Ramachandran P, Iredale JP, Fallowfield JA. Liver fibrosis and repair: immune regulation of wound healing in a solid organ. *Nat Rev Immunol* 2014;14:181–94.

2. Schuppan D, Kim YO. Evolving therapies for liver fibrosis. *J Clin Invest* 2013;123:1887–901.

3. Coombes JD, Swiderska-Syn M, Dollé L, Reid D, Eksteen B, Claridge L, et al. Osteopontin neutralisation abrogates the liver progenitor cell response and fibrogenesis in mice. *Gut* 2015;64:1120–31.

4. Wang X, Lopategi A, Ge X, Lu Y, Kitamura N, Urtasun R, et al. Osteopontin induces ductular reaction contributing to liver fibrosis. *Gut* 2014;63:1805–18.

5. Syn W-K, Agboola KM, Swiderska M, Michelotti GA, Liaskou E, Pang H, et al. NKT-associated hedgehog and osteopontin drive fibrogenesis in non-alcoholic fatty liver disease. *Gut* 2012;61:1323–9.

6. Tacke F, Zimmermann HW. Macrophage heterogeneity in liver injury and fibrosis. *J Hepatol* 2014;60:1090–6.

7. Ramachandran P, Pellicoro A, Vernon MA, Boulter L, Aucott RL, Ali A, et al. Differential Ly-6C expression identifies the recruited macrophage phenotype, which orchestrates the regression of murine liver fibrosis. *Proc Natl Acad Sci* 2012;109:E3186-3195.

8. Ekstedt M, Franzén LE, Mathiesen UL, Thorelius L, Holmqvist M, Bodemar G, et al. Long-term follow-up of patients with NAFLD and elevated liver enzymes. *Hepatology* 2006;44:865–73.

9. Omenetti A, Syn W-K, Jung Y, Francis H, Porrello A, Witek RP, et al. Repair-related activation of hedgehog signaling promotes cholangiocyte chemokine production. *Hepatology* 2009;50:518–27.

10. Ishimura N, Bronk SF, Gores GJ. Inducible Nitric Oxide Synthase Up-Regulates Notch-1 in Mouse Cholangiocytes: Implications for Carcinogenesis. *Gastroenterology* 2005;128:1354–68.

11. Raschke WC, Baird S, Ralph P, Nakoinz I. Functional macrophage cell lines transformed by abelson leukemia virus. *Cell* 1978;15:261–7.

12. Anders S, Pyl PT, Huber W. HTSeq--a Python framework to work with high-throughput sequencing data. *Bioinformatics* 2015;31:166–9.

13. Love MI, Huber W, Anders S. Moderated estimation of fold change and dispersion for RNA-seq data with DESeq2. *Genome Biol* 2014;15:550.

14. Benjamini Y, Hochberg Y. Controlling the False Discovery Rate: A Practical and Powerful Approach to Multiple Testing. *J R Stat Soc Ser B Methodol* 1995;57:289–300.

15. Eden E, Navon R, Steinfeld I, Lipson D, Yakhini Z. GOrilla: a tool for discovery and visualization of enriched GO terms in ranked gene lists. *BMC Bioinformatics* 2009;10:48.

16. Eden E, Lipson D, Yogev S, Yakhini Z. Discovering motifs in ranked lists of DNA sequences. *PLoS Comput Biol* 2007;3:e39.

17. Huang DW, Sherman BT, Lempicki RA. Bioinformatics enrichment tools: paths toward the comprehensive functional analysis of large gene lists. *Nucleic Acids Res* 2009;37:1–13.

18. Huang DW, Sherman BT, Lempicki RA. Systematic and integrative analysis of large gene lists using DAVID bioinformatics resources. *Nat Protoc* 2009;4:44–57.

19. Supek F, Bošnjak M, Škunca N, Šmuc T. REVIGO summarizes and visualizes long lists of gene ontology terms. *PloS One* 2011;6:e21800.

20. Kanehisa M, Sato Y, Kawashima M, Furumichi M, Tanabe M. KEGG as a reference resource for gene and protein annotation. *Nucleic Acids Res* 2016;44:D457-462.

21. Kanehisa M, Goto S. KEGG: Kyoto encyclopedia of genes and genomes. *Nucleic Acids Res* 2000;28:27–30.

22. Mi Z, Guo H, Russell MB, Liu Y, Sullenger BA, Kuo PC. RNA Aptamer Blockade of Osteopontin Inhibits Growth and Metastasis of MDA-MB231 Breast Cancer Cells. *Mol Ther* 2009;17:153–61.

23. Talbot LJ, Mi Z, Bhattacharya SD, Kim V, Guo H, Kuo PC. Pharmacokinetic characterization of an RNA aptamer against osteopontin and demonstration of in vivo efficacy in reversing growth of human breast cancer cells. *Surgery* 2011;150:224–30.

24. Kleiner DE, Brunt EM, Van Natta M, Behling C, Contos MJ, Cummings OW, et al. Design and validation of a histological scoring system for nonalcoholic fatty liver disease. *Hepatology* 2005;41:1313–21.

25. Moylan CA, Pang H, Dellinger A, Suzuki A, Garrett ME, Guy CD, et al. Hepatic gene expression profiles differentiate presymptomatic patients with mild versus severe nonalcoholic fatty liver disease. *Hepatology* 2014;59:471–82.

26. Coombes JD, Choi SS, Swiderska-Syn M, Manka P, Reid DT, Palma E, et al. Osteopontin is a proximal effector of leptin-mediated non-alcoholic steatohepatitis (NASH) fibrosis. *Biochim Biophys Acta* 2016;1862:135–44.

27. Brunt EM, Kleiner DE, Wilson LA, Unalp A, Behling CE, Lavine JE, et al. Portal chronic inflammation in nonalcoholic fatty liver disease (NAFLD): a histologic marker of advanced NAFLD-Clinicopathologic correlations from the nonalcoholic steatohepatitis clinical research network. *Hepatology* 2009 Mar;49(3):809-20.

28. Richardson MM, Jonsson JR, Powell EE, Brunt EM, Neuschwander-Tetri BA, Bhathal PS, et al. Progressive fibrosis in nonalcoholic steatohepatitis: association with altered regeneration and a ductular reaction. *Gastroenterology* 2007;133:80–90.

29. Gadd VL, Melino M, Roy S, Horsfall L, O'Rourke P, Williams MR, et al. Portal, but not lobular, macrophages express matrix metalloproteinase-9: association with the ductular reaction and fibrosis in chronic hepatitis C. *Liver Int* 2013;33:569–79.

30. Anstee QM, Neuschwander-Tetri BA, Wai-Sun Wong V, Abdelmalek MF, Rodriguez-Araujo G, Landgren H, Park GS, Bedossa P, Alkhouri N, Tacke F, Sanyal AJ. Cenicriviroc Lacked Efficacy to Treat Liver Fibrosis in Nonalcoholic Steatohepatitis: AURORA Phase III Randomized Study. *Clin Gastroenterol Hepatol* 2024 Jan;22(1):124-134.e1.

31. Rittling SR. Osteopontin in macrophage function. *Expert Rev Mol Med* 2011;13:e5.

32. Zheng W, Li R, Pan H, He D, Xu R, Guo TB, et al. Role of osteopontin in induction of monocyte chemoattractant protein 1 and macrophage inflammatory protein 1beta through the NF-kappaB and MAPK pathways in rheumatoid arthritis. *Arthritis Rheum* 2009;60:1957–65.

33. Kawashima R, Mochida S, Matsui A, YouLuTuZ Y, Ishikawa K, Toshima K, et al. Expression of osteopontin in Kupffer cells and hepatic macrophages and Stellate cells in rat liver after carbon tetrachloride intoxication: a possible factor for macrophage migration into hepatic necrotic areas. *Biochem Biophys Res Commun* 1999;256:527–31.

34. Kiefer FW, Zeyda M, Gollinger K, Pfau B, Neuhofer A, Weichhart T, et al. Neutralization of osteopontin inhibits obesity-induced inflammation and insulin resistance. *Diabetes* 2010;59:935–46.

35. Cheng J, Huo D-H, Kuang D-M, Yang J, Zheng L, Zhuang S-M. Human macrophages promote the motility and invasiveness of osteopontin-knockdown tumor cells. *Cancer Res* 2007;67:5141–7.

36. Kui Tan T, Zheng G, Hsu T-T, Ra Lee S, Zhang J, Zhao Y, et al. Matrix metalloproteinase-9 of tubular and macrophage origin contributes to the pathogenesis of renal fibrosis via macrophage recruitment through osteopontin cleavage. *Lab Invest* 2013;93:434–49.

FIGURE LEGENDS

Figure 1. A) Cholangiocyte (603B) coexpression of keratin 19 and OPN, relative to RPS9 housekeeping. qPCR product on agarose gel. B) Secretion of OPN by 603B detected by ELISA of conditioned media. *p<0.05. C) Western blot showing short-hairpin knockdown of OPN. D) qRT-PCR detection of chemokines CCL2, CXCL1 and CCL5 with OPN knockdown. E) Cytometric bead array detection of chemokines secreted in 603B conditioned media. *p<0.05 shOPN vs shScr; unpaired t-test with Welch correction.

Figure 2. A) NF-κB activity detected by TransAM® DNA-binding ELISA of family subunits. Lysates from shScr and shOPN 603B cholangiocytes are compared to quantify transcription factor activation and the specific NF-κB subunit. Activity (a.u. Mean±SD) shown, shOPN vs shScr unpaired t-test with Welch correction. B) Western blot visualizing equivalent total protein levels of p65 and α-actinin used as loading control.

Figure 3. Macrophage activity. Transmigration assays: RAW264.7 macrophages exposed to conditioned media from 603B cholangiocytes. Number of migrated cells shown. Conditioned media was treated with several schemes: A) control IgG, OPN-neutralizing antibody, chemokine-neutralizing antibodies (against CCL2/MCP1, CXCL1/KC and CCL5/RANTES) and recombinant OPN; B) sham aptamer, OPN-neutralizing aptamer and recombinant OPN; C) conditioned media from shScr and shOPN 603B cholangiocytes. D) Macrophage expression of activation markers Class II MHC Transactivator (Ciita) and Arginase 1 (Arg1) after treatment with conditioned media from shScr or shOPN 603B cholangiocytes. qRT-PCR data shown, Mean±SD, p<0.05, shOPN vs shScr, unpaired t-test with Welch correction.

Figure 4. Murine liver injury models treated with OPN-neutralizing aptamer. A) Liver injury (ALT) and fibrogenesis markers (αSMA and Col1a1). *p<0.05. B) Sirius red histology for fibrosis *p<0.05, unpaired t-test with Welch correction. C) Chemokine mRNA levels by qRT-PCR analysis whole liver tissue from MCD-model and CCl4-model mice. *p<0.05 vs Normal, **p<0.05 vs Sham aptamer+MCD, unpaired t-test with Welch correction.

Figure 5. Accumulation of inflammatory monocytes in murine liver injury. MCD model shown. A) Immunohistochemical detection of macrophages labelled by the F4/80 marker with brown chromogen. B) Flow cytometric analysis of inflammatory monocyte subsets from total liver, gated on $CD11b^{+}F4/80^{+}$. The Ly-6C antigen was used to distinguish 'pro-fibrogenic' Ly-$6C^{High}$ monocytes and 'restorative' Ly-$6C^{Low}$ monocytes. *p<0.05 vs sham, unpaired t-test with Welch correction.

Figure 6. Human MASH. A) Inflammatory monocyte accumulation detected by CD68 immunohistochemistry of MASH versus normal liver. B) Progression from early to advanced MASH is accompanied by increased OPN and chemokines IL-8 and CCL2. Microarray data shown. P<0.05 Advanced MASH vs Early MASH. C) Dual immunohistochemistry with cholangiocyte marker CK19 (green) and OPN (brown) in normal liver and MASH. Quantification of double positive cells is shown, including the proportion of $CK19^{+}$ cells that are also OPN^{+}. Mean±SD; *p<0.05, unpaired t-test with Welch correction.

Figure 1

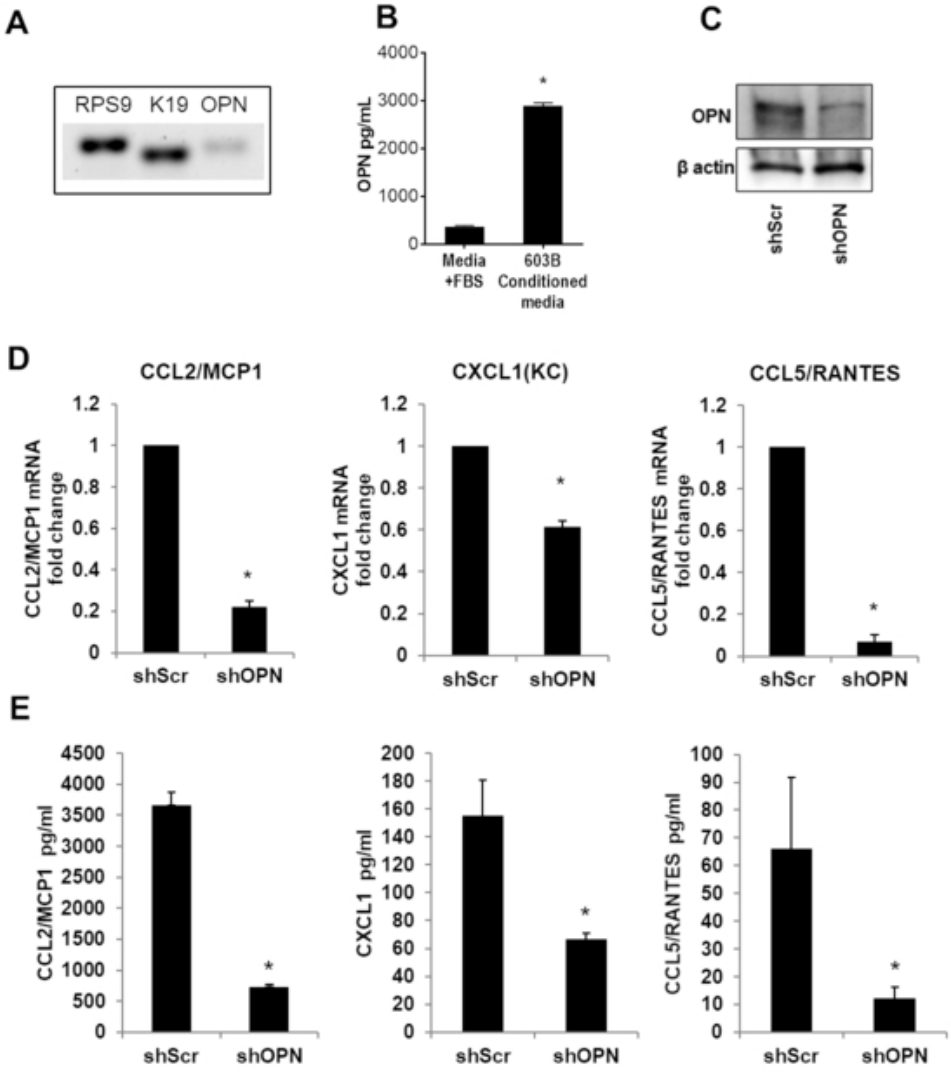

48x57mm (300 x 300 DPI)

Figure 2. OPN loss alters NF-κB signalling

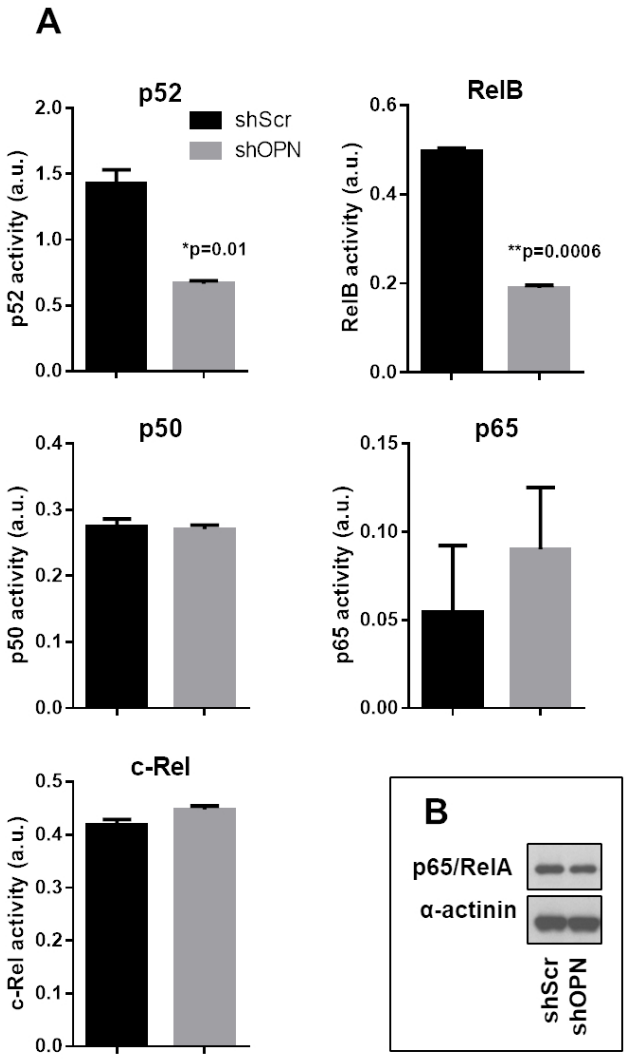

63x107mm (300 x 300 DPI)

Figure 3. OPN loss in cholangiocytes reduces macrophage transmigration and alters macrophage activation phenotype

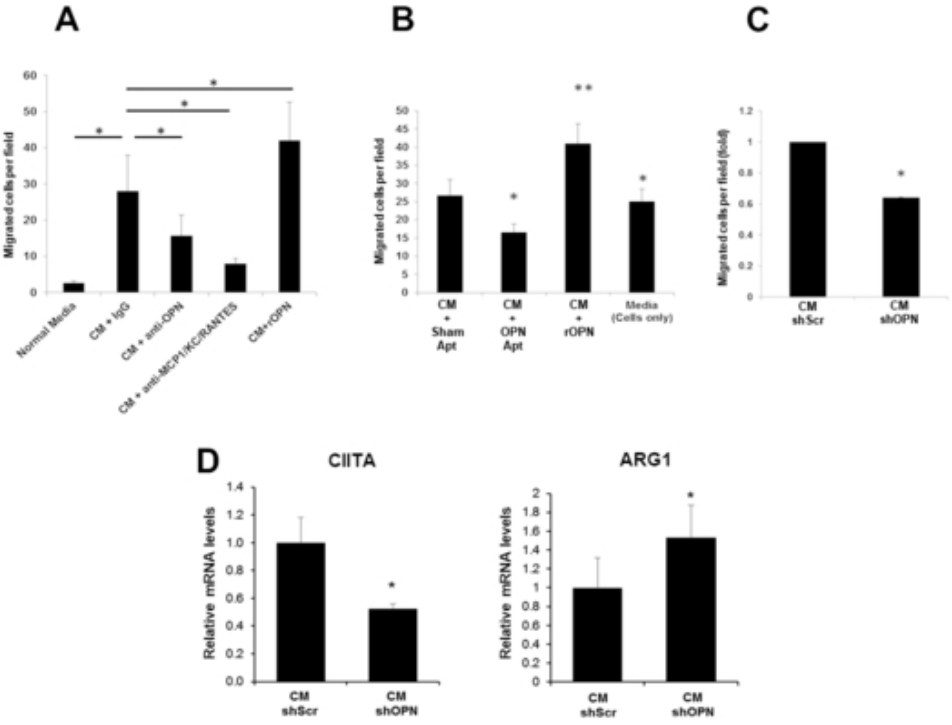

46x41mm (300 x 300 DPI)

Figure 4. OPN neutralization supresses injury and fibrosis in vivo, and reduces expression of chemokines CCL2/MCP-1, CXCL1/KC and CCL5/RANTES

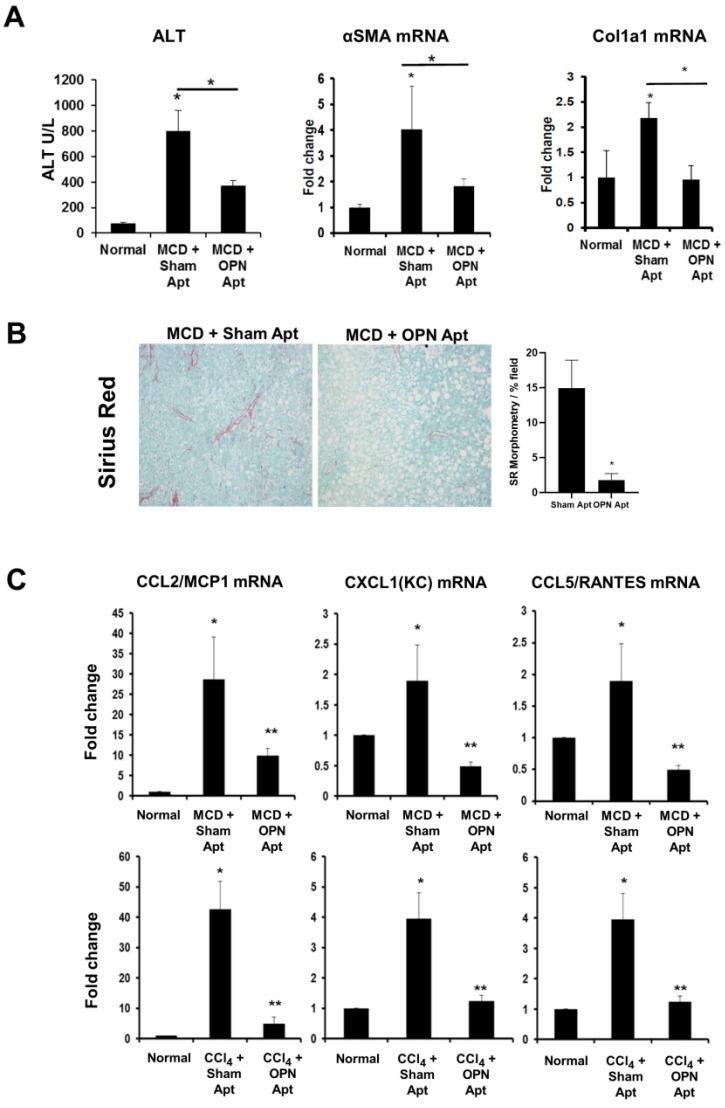

163x258mm (300 x 300 DPI)

Figure 5. OPN neutralization in vivo suppresses macrophage accumulation

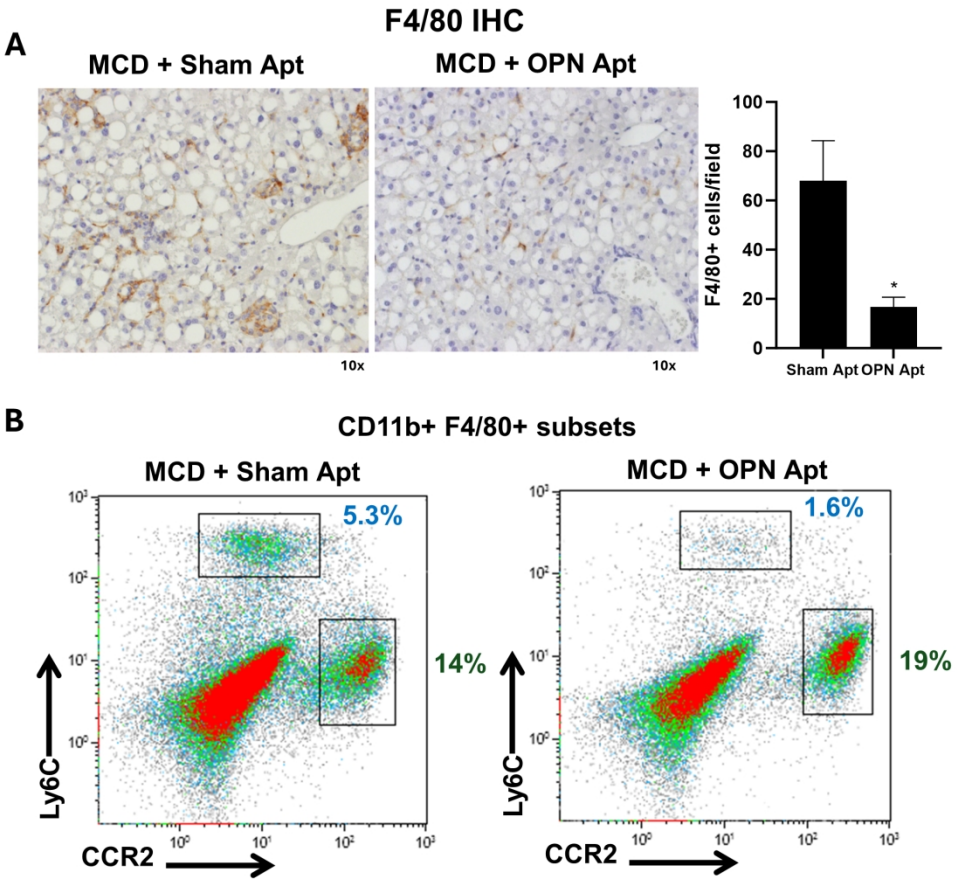

183x176mm (300 x 300 DPI)

Figure 6. Human MASH

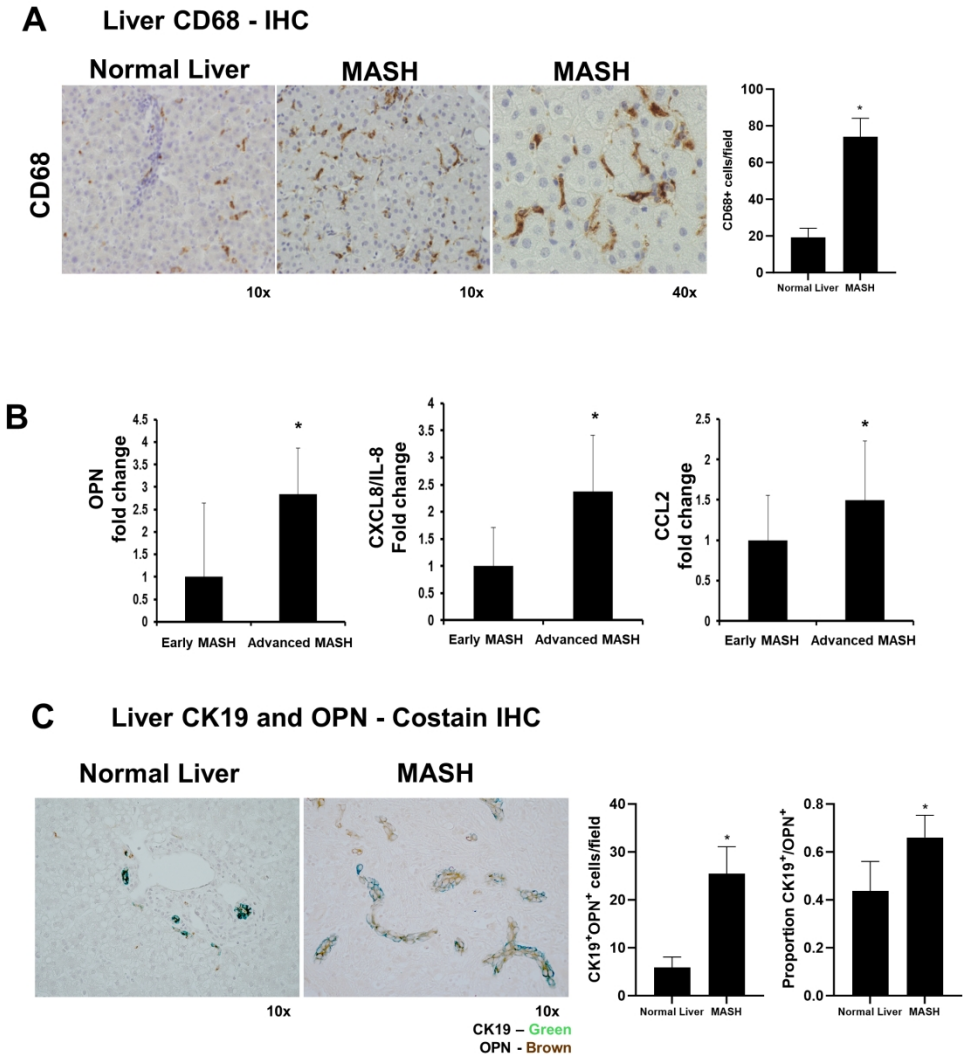

186x218mm (300 x 300 DPI)

Table 1. Differential expression of chemokines detected by RNAseq†

Gene ID	base Mean	log2Fold Change	lfcSE	p_{adj}
CXCL16	165.15	-2.708	0.265	1.79E-21*
CXCL11	131.84	-2.271	0.272	3.14E-14*
CXCL110	2259.20	-1.850	0.212	1.65E-15*
CCL5 (RANTES)	30.39	-1.419	0.274	2.05E-05*
CCL2 (MCP-1)	4437.61	-1.343	0.227	4.21E-07*
CCL9	34.34	-1.169	0.275	0.00095*
CCL7	141.57	-1.139	0.280	0.00194*
CXCL1 (KC, Fsp, Gro1)	550.42	-1.030	0.233	0.00051*
CX3CL1 (Fractalkine)	306.73	-1.006	0.225	0.00042*
CXCL5	462.74	-0.987	0.232	0.00098*
CCL8	21.93	-0.670	0.261	0.12296
CCL20 (MIP3A)	726.26	-0.545	0.236	0.19727
CCL17	182.68	-0.472	0.247	0.35222
CCL6	10.71	-0.327	0.229	0.57309
CXCL12	11.62	0.233	0.235	0.75865
CCL25	311.05	0.192	0.224	0.80567
CCL28	10.66	0.089	0.208	0.92633

†All Chemokines detected by RNAseq shown.
baseMean = expression level as indicated by reads across all replicates
log2FoldChange = log2 fold change between the groups; shOPN vs control.
lfcSE = standard error of the log2FoldChange
p_{adj} = *P* value adjusted for multiple testing using Benjamini-Hochberg procedure.
*Significance indicated at $p<0.05$.

Supplemental Methods

Semi-quantitative real-time PCR

Total RNA was extracted from cell cultures or liver tissue using a standard TRIzol® technique (Life Technologies, Carlsbad, CA). cDNA templates were reverse transcribed from RNA (1 µg) using an iScript kit (Bio-Rad). cDNA (25 ng) was amplified using SYBR® Green PCR Master Mix (Life Technologies) and target-specific oligonucleotide primers on an Applied Biosystems 7500 Real-Time PCR system. Threshold cycles (Ct) were calculated automatically by the system software and target gene levels determined using the 2–ΔΔCt method, relative to the S9 ribosomal protein housekeeping gene. Primer sequences are listed in ***Supplemental Table 1***. Samples were taken from three independently prepared extracts.

Agarose gel electrophoresis

Select PCR products were mixed with 5x DNA Electrophoresis sample loading dye (Bio-Rad, Hercules, CA) and electrophoresed in 2% w/v high-resolution agarose (UltraPure™ Agarose 1000, Life Technologies, Carlsbad, CA) in tris-borate EDTA. Gels were stained with GelRed® Nucleic Acid Gel stain (Biotium, Fremont, CA) and photographed on a on a Bio-Rad ChemiDoc MP imaging system.

Western blot

Cell cultures were lysed in cold RIPA buffer (pH 7.4, 50 mM Tris-HCl, 150 mM NaCl, 1mM EDTA, 1% NP-40, 0.01% SDS) with Protease Inhibitor Cocktail Tablets (Roche, Indianapolis, IN) and phosphatase inhibitors (1 mM Na_3VO_4, 1 mM NaF). Protein concentration was measured by the Precision Red Advanced Protein Assay (Cytoskeleton Inc., Denver, CO). Approximately 15 µg protein was loaded on precast acrylamide gels (Mini-PROTEAN® TGX™ Bio-Rad, Hercules, CA), and electro-transferred to nitrocellulose or PVDF membranes (0.45 µm, Life Technologies). Membranes were blocked in Bløk-CH Noise Cancelling Reagent (Merck-Millipore, Temecula, CA) and incubated with primary antibodies listed in ***Supplemental Table 2*** overnight at 4°C. After washing, ECL™ donkey anti-rabbit, ECL™sheep anti-mouse (GE Life Sciences, Amersham, UK) or rabbit-anti goat (Santa Cruz, Dallas, TX) HRP-conjugated secondary antibodies were added at 1:20,000 dilution in TBST. Clarity Western ECL Reagent (Bio-Rad) substrate was used to visualize specific antibody-HRP complexes on a Bio-Rad ChemiDoc MP imaging system. Loading equivalence was determined using β-actin detection (Sigma, St. Louis, MO). Band density was measured using the peak analysis tool of NIH Image J version 1.47f (Schneider et al., 2012, https://doi.org/10.1038/nmeth.2089).

Histopathology and immunohistochemistry

Immunohistochemical staining was performed as previously described [3] to detect OPN, αSMA, F4/80, CD68 and CK19 utilising the DAKO Envision System (DAKO Corporation) according to the manufacturer's protocol. Briefly, sections were de-paraffinized in xylene, dehydrated in ethanol, and incubated with 3% hydrogen peroxide to block endogenous peroxidase. Antigen retrieval was performed by heating in 10 mM sodium citrate buffer (pH 6.0) or incubating with pepsin (Invitrogen). Sections were blocked in DAKO protein block (DAKO), followed by incubation with primary antibodies listed in ***Supplemental Table 2***. Target proteins were visualized using HRP-conjugated secondary antibody and DAB chromogen (anti-rabbit, K4003; anti-mouse, K4001; DAB reagent, K3466; DAKO) and sections counterstained with Aqua Hematoxylin (Innovex Biosciences). For double-immunohistochemistry, the additional target was detected using Vina Green Chromogen Kit (Bio-Care Medical, Pacheco, CA). Negative controls constituted sections exposed to 1% bovine serum albumin instead of the respective primary antibodies. Quantitation was performed on a minimum of 10 nonoverlapping fields and counted via ImageJ. Sirius red histology and morphometry was also as per previously described [ref. 3].

Human histopathology was evaluated by an independent pathologist at Duke University Medical Center using assessment criteria as per the NASH (MASH) Clinical Research Network scoring system, assessing indicative histological features including Steatosis (grade 0-3), Lobular Inflammation (grade 0-3), Portal inflammation (grade 0-1), Ballooning (0-2), Fibrosis (stage 0-4), and Portal fibrosis (grade 0-1, stage 1c, 2, 3 and 4) [ref. 24].

Supplemental Methods

Semi-quantitative real-time PCR

Total RNA was extracted from cell cultures or liver tissue using a standard TRIzol® technique (Life Technologies, Carlsbad, CA). cDNA templates were reverse transcribed from RNA (1 µg) using an iScript kit (Bio-Rad). cDNA (25 ng) was amplified using SYBR® Green PCR Master Mix (Life Technologies) and target-specific oligonucleotide primers on an Applied Biosystems 7500 Real-Time PCR system. Threshold cycles (Ct) were calculated automatically by the system software and target gene levels determined using the 2–ΔΔCt method, relative to the S9 ribosomal protein housekeeping gene. Primer sequences are listed in ***Supplemental Table 1***. Samples were taken from three independently prepared extracts.

Agarose gel electrophoresis

Select PCR products were mixed with 5x DNA Electrophoresis sample loading dye (Bio-Rad, Hercules, CA) and electrophoresed in 2% w/v high-resolution agarose (UltraPure™ Agarose 1000, Life Technologies, Carlsbad, CA) in tris-borate EDTA. Gels were stained with GelRed® Nucleic Acid Gel stain (Biotium, Fremont, CA) and photographed on a on a Bio-Rad ChemiDoc MP imaging system.

Western blot

Cell cultures were lysed in cold RIPA buffer (pH 7.4, 50 mM Tris-HCl, 150 mM NaCl, 1mM EDTA, 1% NP-40, 0.01% SDS) with Protease Inhibitor Cocktail Tablets (Roche, Indianapolis, IN) and phosphatase inhibitors (1 mM Na_3VO_4, 1 mM NaF). Protein concentration was measured by the Precision Red Advanced Protein Assay (Cytoskeleton Inc., Denver, CO). Approximately 15 µg protein was loaded on precast acrylamide gels (Mini-PROTEAN® TGX™ Bio-Rad, Hercules, CA), and electro-transferred to nitrocellulose or PVDF membranes (0.45 µm, Life Technologies). Membranes were blocked in Bløk-CH Noise Cancelling Reagent (Merck-Millipore, Temecula, CA) and incubated with primary antibodies listed in ***Supplemental Table 2*** overnight at 4°C. After washing, ECL™ donkey anti-rabbit, ECL™sheep anti-mouse (GE Life Sciences, Amersham, UK) or rabbit-anti goat (Santa Cruz, Dallas, TX) HRP-conjugated secondary antibodies were added at 1:20,000 dilution in TBST. Clarity Western ECL Reagent (Bio-Rad) substrate was used to visualize specific antibody-HRP complexes on a Bio-Rad ChemiDoc MP imaging system. Loading equivalence was determined using β-actin detection (Sigma, St. Louis, MO). Band density was measured using the peak analysis tool of NIH Image J version 1.47f (Schneider et al., 2012, https://doi.org/10.1038/nmeth.2089).

Histopathology and immunohistochemistry

Immunohistochemical staining was performed as previously described [3] to detect OPN, αSMA, F4/80, CD68 and CK19 utilising the DAKO Envision System (DAKO Corporation) according to the manufacturer's protocol. Briefly, sections were de-paraffinized in xylene, dehydrated in ethanol, and incubated with 3% hydrogen peroxide to block endogenous peroxidase. Antigen retrieval was performed by heating in 10 mM sodium citrate buffer (pH 6.0) or incubating with pepsin (Invitrogen). Sections were blocked in DAKO protein block (DAKO), followed by incubation with primary antibodies listed in ***Supplemental Table 2***. Target proteins were visualized using HRP-conjugated secondary antibody and DAB chromogen (anti-rabbit, K4003; anti-mouse, K4001; DAB reagent, K3466; DAKO) and sections counterstained with Aqua Hematoxylin (Innovex Biosciences). For double-immunohistochemistry, the additional target was detected using Vina Green Chromogen Kit (Bio-Care Medical, Pacheco, CA). Negative controls constituted sections exposed to 1% bovine serum albumin instead of the respective primary antibodies. Quantitation was performed on a minimum of 10 nonoverlapping fields and counted via ImageJ. Sirius red histology and morphometry was also as per previously described [ref. 3].

Human histopathology was evaluated by an independent pathologist at Duke University Medical Center using assessment criteria as per the NASH (MASH) Clinical Research Network scoring system, assessing indicative histological features including Steatosis (grade 0-3), Lobular Inflammation (grade 0-3), Portal inflammation (grade 0-1), Ballooning (0-2), Fibrosis (stage 0-4), and Portal fibrosis (grade 0-1, stage 1c, 2, 3 and 4) [ref. 24].

Supplemental Figure 1.

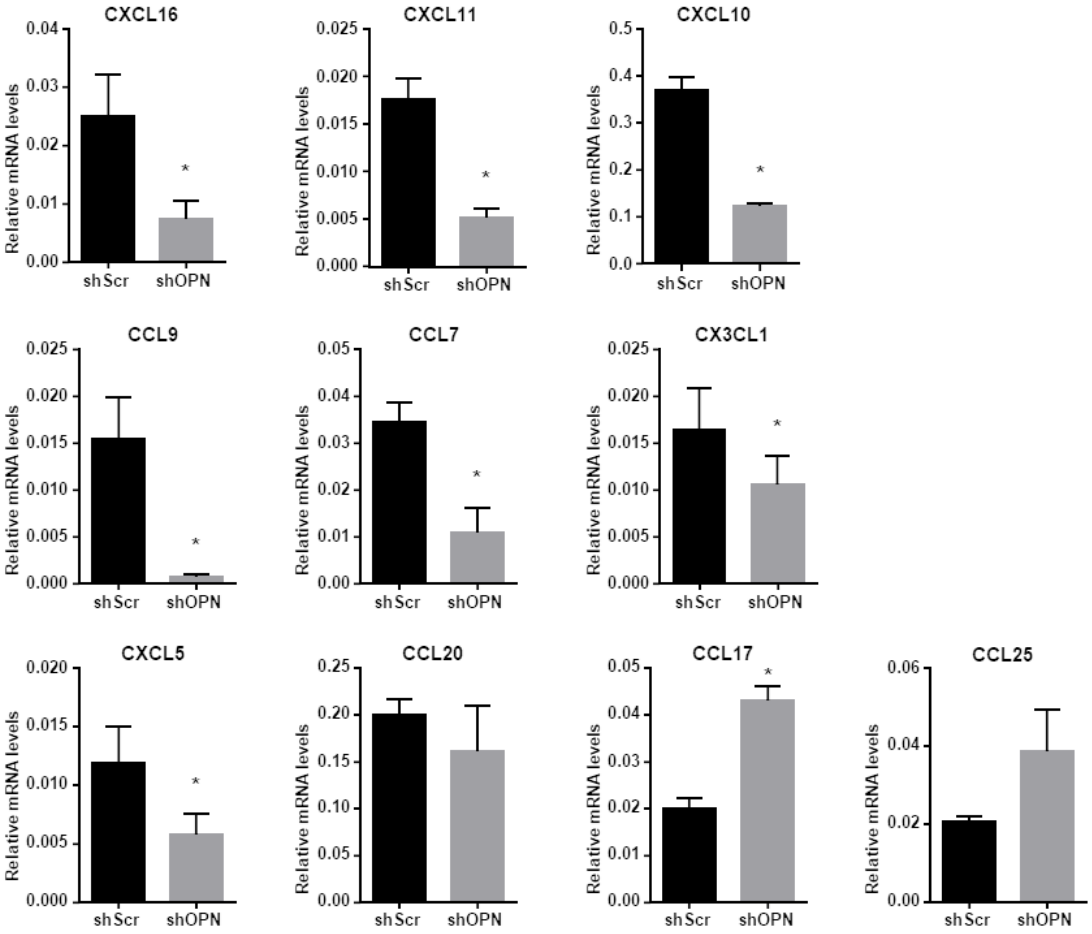

Supplemental Figure 1. Verification of altered chemokine expression. The chemokines detected by RNAseq analysis, including those that were significantly downregulated, were subjected to qRT-PCR. shScr vs shOPN cholangiocytes shown. Three replicate samples for analysis were extracted independently of mRNA used for RNAseq.

Supplemental Figure 2.

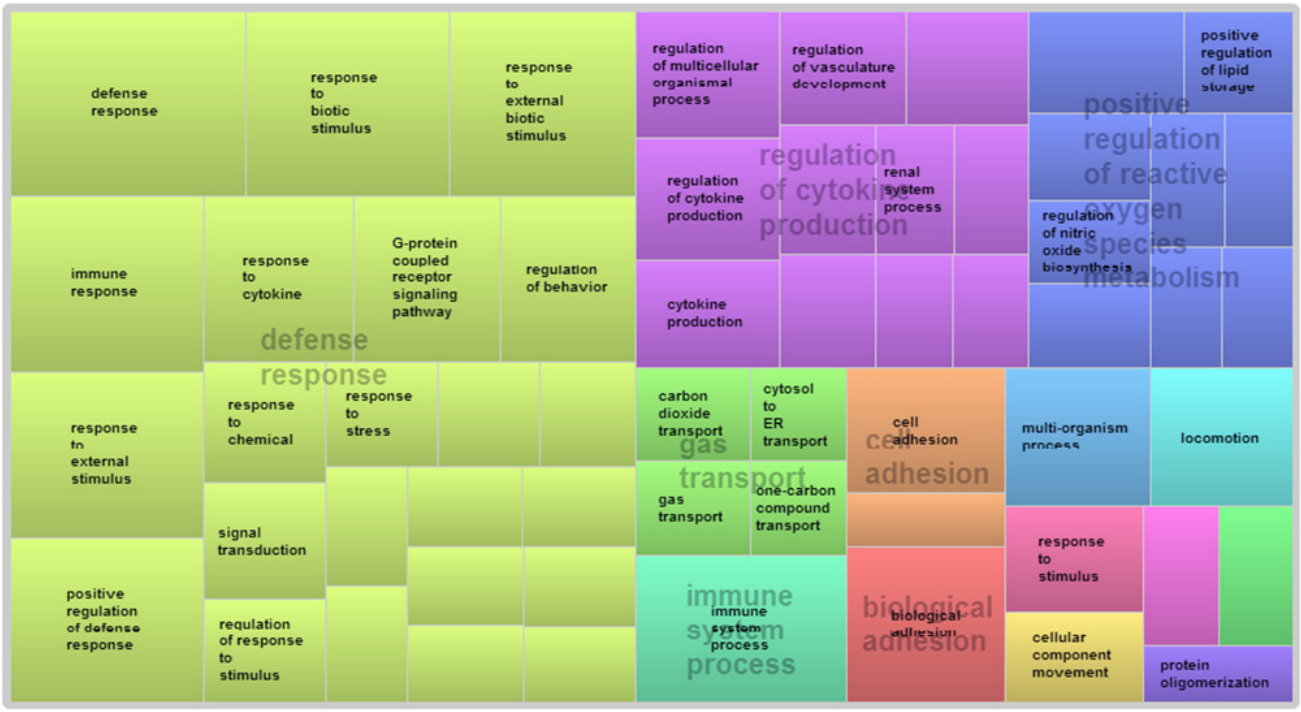

Supplemental Figure 2. Functional groupings of enriched gene ontologies. To reduce redundancy between functionally overlapping terms, RNAseq-based gene ontology data from GOrilla was filtered using ReviGO to generate functionally meaningful groups. Functional groupings shown are altered with loss of OPN in cholangiocytes. Colour represents common functional grouping and box size is proportional to the number of genes affected.

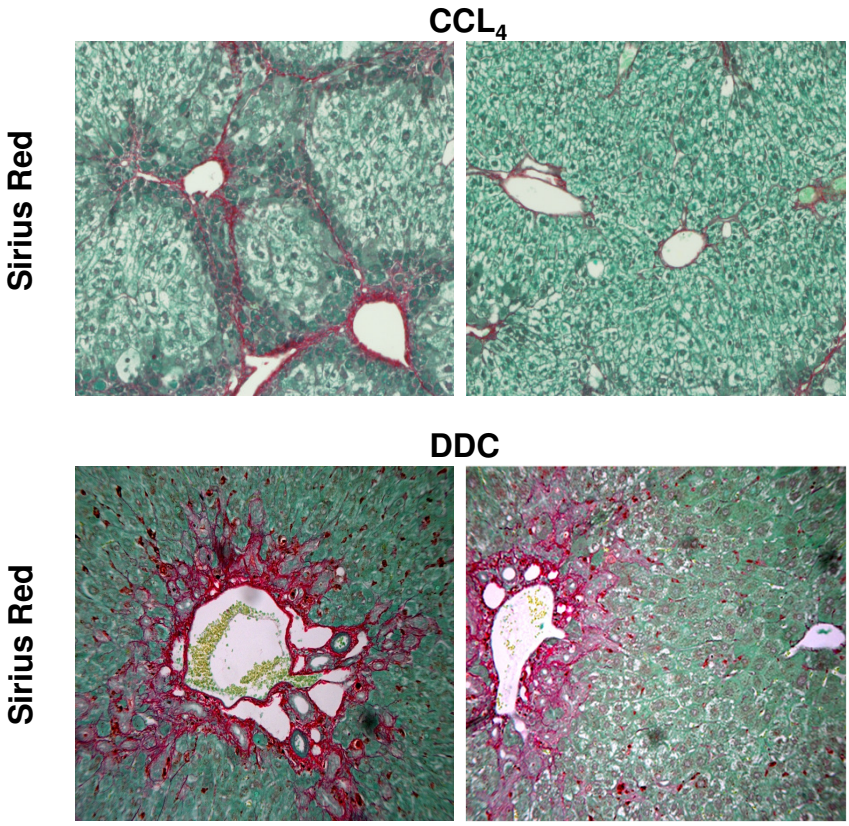

Supplemental Figure 3. Sirius red histology. OPN-neutralization ameliorates fibrosis in murine CCl4 and DDC models. Animals were treated with sham aptamer (left column) or OPN-specific neutralizing aptamer (right column).

Supplemental Figure 4.

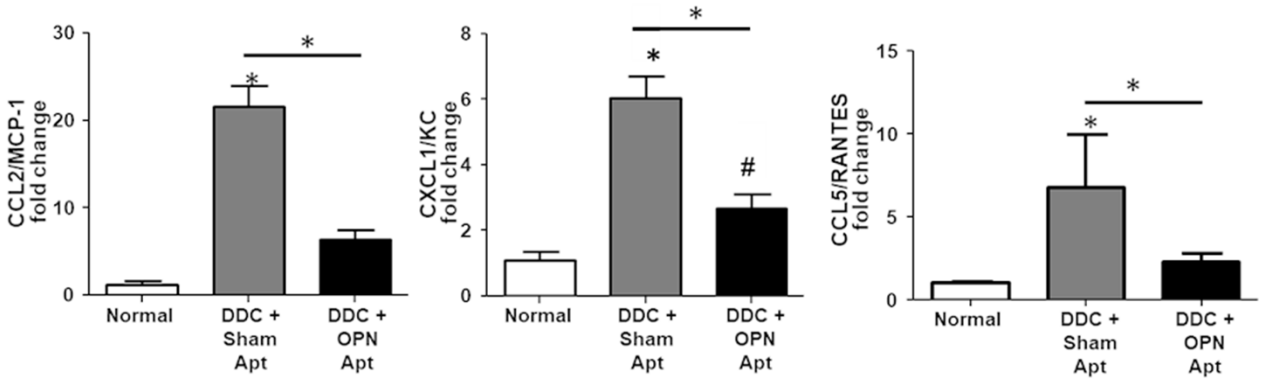

Supplemental Figure 4. DDC Model. Chemokine mRNA levels by qRT-PCR analysis of whole liver tissue from DDC-model mice.

Supplemental Figure 5.

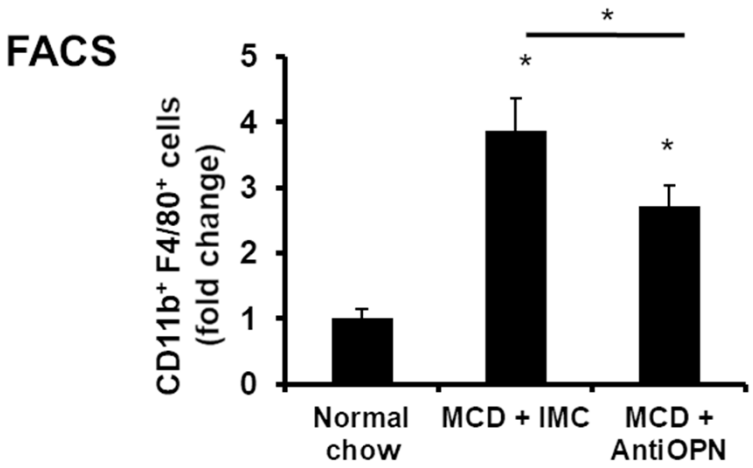

Supplemental Figure 5. Flow cytometric detection of inflammatory monocytes/macrophages labelled by CD11b+F4/80+ from total liver of of a 5-week MCD murine model. MCD mice were injected either control (IgG) or anti-OPN (R&D) in the final week, (n=5/group four injections; 50 µg/injection), a dose demonstrated to reduce fibrosis (Coombes et al., 2015), and sacrificed 24 h after the final injection. Data presented as fold change relative to livers from normal fed mice.

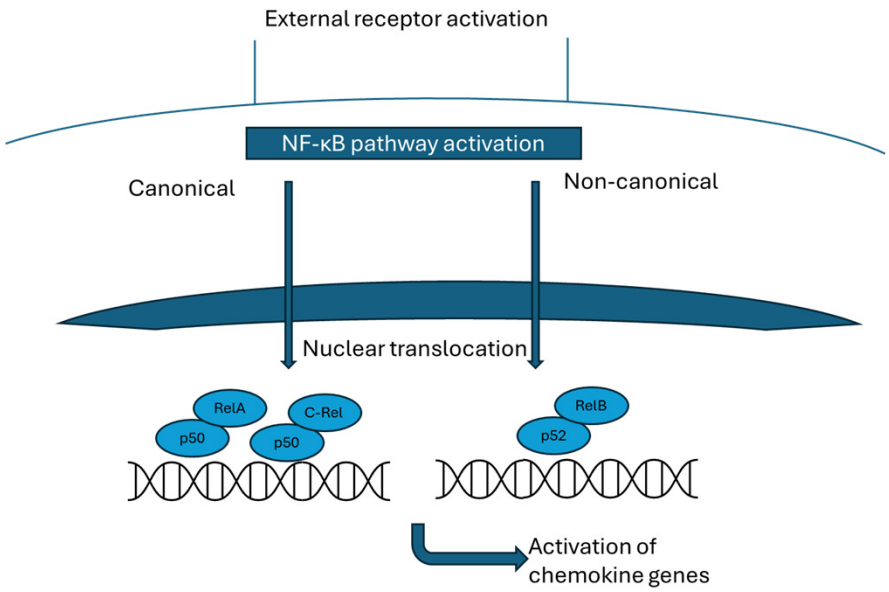

Supplemental Figure 6. Schematic representation of NF-kB pathway activation, delineating differences in canonical vs non-canonical branches. Translocation of active p50-RelA and p50-c-Rel heterodimer complexes (and p50 homodimers) to the nucleus are consistent with the canonical branch, whereas the active p52-RelB heterodimer distinguishes the non-canonical branch. Non-canonical signaling is generally considered slower, more persistent and has been associated with chronic inflammatory conditions, whereas canonical activation is rapid and transient, typically present in circumstances such as infection and acute injury

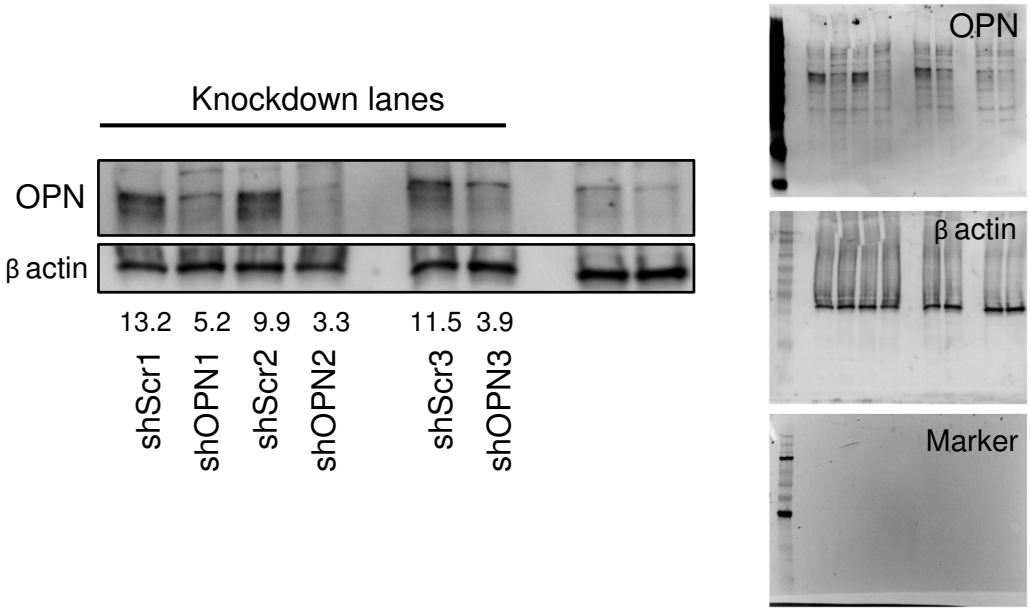

Supplemental Figure 7. Western Bot quantitation is shown for OPN knockdown. Grey intensity was plotted and the resulting area under curve plotted to generate to generate lane intensity values. Values were corrected for loading by β actin. Source blot membranes are shown. Cell lysates were taken from three independent extracts. Average shOPN knockdown value by protein level is approximately 65%.

Supplemental Table 1. List of primer pairs for qRT-PC

Target (Mouse)	Forward 5'->3'	Reverse 5'->3'
RPS9	AGCCGGCCTAGCGAGGTCAA	CGAAGGGTCTCCGTGGGGTCA
OPN (Spp1)	TGGCAGCTCAGAGGAGAAGAAGC	GGGTCAGGCACCAGCCATGTG
Collagen1a1	AATGGCACGGCTGTGTGCGA	AGCACTCGCCCTCCCGTCTT
K19	GTGAAGATCCGCGACTGGT	AGGCGAGCATTGTCAATCTG
αSMA (ACTA2)	GATGAAGCCCAGAGCAAGAG	CTTTTCCATGTCGTCCCAGT
CXCL16	TGAACTAGTGGACTGCTTTGAGC	GCAAATGTTTTTGGTGGTGA
CXCL11	AAAGTCACGTGCACACTCCA	CACTGGTCCGGATTGCAGTA
CXCL10	ATGACGGGCCAGTGAGAATG	TCAACACGTGGGCAGGATAG
CCL9	ATCAGCAAGAGGGGGTTCCA	AGGTCCGTGGTTGTGAGTTT
CCL7	GTGTCCCTGGGAAGCTGTTA	ATAGCCTCCTCGACCCACTT
CX3CL1	AACTTCCGAGGCACAGGATG	AGATGTCAGCCGCCTCAAAA
CXCL5	TTCTGTTGCTGTTCACGCTG	AAGCAAACACAACGCAGCTC
CCL20	CGACTGTTGCCTCTCGTACA	AGCTTCATCGGCCATCTGTC
CCL17	ACTTCAAAGGGGCCATTCCT	TGCCCTGGACAGTCAGAAAC
CCL25	AACCCCAACAGTACAAGCGT	TGTTGGTCTTTCTGGGCATCA
CIITA	CTTCATAGAGCACATTGGAGCAG	GCGTCTCTTCTGAGGCTTCTGT
Arg1	TTCGGAACTCAACGGGAGG	CATGTGGCGCATTCACAGTC

Supplemental Table 2. List of Antibodies

Antibody	Application	Supplier	Catalog/Clone
αSMA	IHC	Abcam	ab32575
CK19	IHC/Western	Abcam	ab15463
F4/80	IHC	AbDSerotec	MCA497GA
p65	Western	Santa Cruz	4H211
α-actinin	Western	Santa Cruz	sc-7454-R
β actin	Western	Sigma	AC-74
CD11b	FC	BD	M1/70
CCR2	FC	R&D	FAB5538
Ly-6C	FC	BD	AL-21
F4/80	FC	eBioscience	FAB5580
CD68	IHC	Dako	M0876
CCL2 (MCP1)	Neutralization	R&D	MAB479
CCL5/RANTES	Neutralization	R&D	MAB478
CXCL1/KC	Neutralization	R&D	MAB453
IgG	Neutralization	Abcam	6-001-F
Osteopontin	Neutralization/Western/IHC	R&D	AF808

Supplemental Table 3. Most-enriched functional gene ontologies based on differentially expressed genes.[a]

GOrilla software		
GO Term	**Description**	**P-value**[b]
GO:0006952	defense response	2.84E-16
GO:0043207	response to external biotic stimulus	3.16E-14
GO:0009607	response to biotic stimulus	3.82E-14
GO:0006955	immune response	5.55E-13
GO:0098542	defense response to other organism	9.71E-13
GO:0034341	response to interferon-gamma	2.33E-12
GO:0009605	response to external stimulus	2.53E-12
GO:0002376	immune system process	3.07E-12
GO:0031349	positive regulation of defense response	4.08E-12
GO:0071346	cellular response to interferon-gamma	4.68E-12
GO:0051707	response to other organism	4.75E-12
GO:0031347	regulation of defense response	8.19E-11
GO:0006954	inflammatory response	1.21E-10
GO:0034097	response to cytokine	2.03E-10
GO:0007186	G-protein coupled receptor signaling pathway	4.63E-10
GO:0002682	regulation of immune system process	6.35E-10
GO:0006935	chemotaxis	8.65E-10
GO:0022610	biological adhesion	9.51E-10
GO:0048247	lymphocyte chemotaxis	1.11E-09
GO:0042330	taxis	1.15E-09
GO:0071345	cellular response to cytokine stimulus	1.65E-09
GO:0002687	positive regulation of leukocyte migration	2.42E-09
GO:0002684	positive regulation of immune system process	4.12E-09
GO:0050795	regulation of behavior	6.03E-09
GO:0048520	positive regulation of behavior	6.46E-09
GO:0070098	chemokine-mediated signaling pathway	7.49E-09
GO:0072676	lymphocyte migration	7.94E-09
GO:0042742	defense response to bacterium	1.00E-08
GO:0050920	regulation of chemotaxis	1.60E-08
DAVID software		
GO Term	**Description**	**P-value**[c]
GO:0006955	immune response	1.71E-08
GO:0008009	chemokine activity	4.10E-06
GO:0042379	chemokine receptor binding	5.17E-06
GO:0006935	chemotaxis	6.56E-05
GO:0042330	taxis	6.56E-05
GO:0048002	antigen processing and presentation of peptide antigen	1.29E-04
GO:0030029	actin filament-based process	2.62E-04
GO:0005096	GTPase activator activity	3.34E-04
GO:0005125	cytokine activity	4.75E-04
GO:0002478	antigen processing and presentation of exogenous peptide antigen	8.16E-04
GO:0060589	nucleoside-triphosphatase regulator activity	9.00E-04
GO:0008047	enzyme activator activity	9.67E-04
GO:0030036	actin cytoskeleton organization	1.23E-03
GO:0022402	cell cycle process	1.51E-03
GO:0030695	GTPase regulator activity	1.56E-03
GO:0005886	plasma membrane	1.79E-03
GO:0019884	antigen processing and presentation of exogenous antigen	2.08E-03
GO:0008092	cytoskeletal protein binding	2.25E-03
GO:0019882	antigen processing and presentation	2.38E-03
GO:0007626	locomotory behavior	2.68E-03
GO:0070161	anchoring junction	2.95E-03
GO:0044459	plasma membrane part	3.06E-03
GO:0046983	protein dimerization activity	3.36E-03
GO:0032088	negative regulation of NF-kappaB transcription factor activity	3.68E-03

These lists display the most enriched functional gene clusters, generated from the full list of differentially expressed genes. [a]Functional clusters were identified using two differing algorithms; GOrilla and DAVID. The most enriched GO terms for each method are shown. Based on differentially expressed genes from RNAseq data comparing shNS and shOPN cholangiocytes. [b]P-value based on minimum hypergeometric statistics test for enrichment of GO terms from a ranked gene list. [c]P-value based on Fisher's exact test. Smaller values are more enriched.

Supplemental Table 4. Pathways most affected by OPN-knockdown in cholangiocytes.

KEGG Pathway	Count[a]	PValue[b]	Genes	Fold Enriched	Benjamini[c]
mmu04621 *NOD-like receptor signaling pathway*	10	2.79E-04	CXCL1, NOD2, HSP90AA1, CCL2, MAPK12, IL18, NFKBIA, CCL5, BIRC3, CCL7	4.56	0.045263
mmu04060 *Cytokine-cytokine receptor interaction*	20	8.86E-04	CXCL1, EGFR, BMP2, CCL2, CXCL5, CSF1, IL18, TNFSF15, CCL9, CX3CL1, CXCL11, CCL5, CCL7, CXCL10, TNFRSF9, CXCL16, IL5RA, FAS, IL13RA1, FIGF	2.32	0.070964
mmu04062 *Chemokine signaling pathway*	15	0.004663	CXCL1, CCL2, CXCL5, GNAI1, CCL9, NFKBIA, CX3CL1, CXCL11, CCL5, CCL7, CXCL10, GNG10, CXCL16, JAK2, GRK5	2.33	0.227889
mmu04623 *Cytosolic DNA-sensing pathway*	7	0.012182	DDX58, POLR3G, TMEM173, IL18, NFKBIA, CCL5, CXCL10	3.60	0.398703
mmu04620 *Toll-like receptor signaling pathway*	9	0.022732	FOS, MAPK12, IRF5, TLR2, NFKBIA, CCL5, CXCL11, CXCL10, SPP1	2.57	0.533931
mmu04010 *MAPK signaling pathway*	17	0.023799	EGFR, CACNA2D1, TAOK3, MAPKAPK3, FGF13, NFKB2, STK3, FOS, ATF4, MAPK12, RPS6KA2, JUND, PLA2G6, MAPK8IP1, FAS, MAP3K14, MAP3K12	1.81	0.486441
mmu05200 *Pathways in cancer*	19	0.03463	EGFR, TRAF1, WNT10A, BMP2, TCF7, HSP90AA1, PTGS2, MMP9, ARNT2, NFKBIA, FGF13, NFKB2, BIRC3, COL4A6, RBX1, FOS, EP300, FAS, FIGF	1.66	0.566467
mmu04612 *Antigen processing and presentation*	8	0.040484	H2-K1, HSP90AA1, H2-M2, TAP2, TAP1, H2-D1, CD74, B2M	2.48	0.575784
mmu04622 *RIG-I-like receptor signaling pathway*	6	0.090273	DDX58, TMEM173, ISG15, MAPK12, NFKBIA, CXCL10	2.49	0.825362

This list of pathways is generated from the full list of differentially expressed genes, displaying the most altered pathway clusters.

[a] number of genes affected in pathway

[b] Modified Fisher Exact P-Value. Smaller values are more enriched

[c] Benjamini-Hochsberg adjusted for multiple comparisons

Supplemental Table 5. Differentially expressed NF-κB target genes and family genes[†π].

Gene ID	base Mean	log2Fold Change	lfcSE	p_{adj}
NF-κB target genes				
C3	3020.974	-5.664	0.212	1.217E-152
Mmp9	220.225	-3.515	0.262	1.546E-37
Slfn2	77.558	-2.296	0.286	3.596E-13
Xdh	429.714	-2.162	0.237	4.917E-17
Nod2	59.432	-1.692	0.287	5.023E-07
S100a4	974.385	-1.601	0.197	1.868E-13
Plau	153.106	-1.437	0.281	2.726E-05
Tnfrsf9	88.479	-1.421	0.280	3.024E-05
Vcam1	1723.971	-1.409	0.219	2.306E-08
Birc3	509.968	-1.395	0.218	2.805E-08
Ptgs2	139.489	1.287	0.268	1.098E-04
Tlr2	467.095	-1.140	0.214	1.003E-05
Tap1	78.363	-1.114	0.287	3.704E-03
Tnfsf15	131.928	-0.939	0.263	9.860E-03
Lsp1	34.525	-0.901	0.282	2.980E-02
Upk1b	61.931	-0.891	0.287	3.768E-02
Tnip3	25.034	-0.870	0.273	3.008E-02
Traf1	139.397	-0.859	0.278	3.879E-02
Slc11a2	1503.458	-0.837	0.214	3.370E-03
Ptgds	2271.977	-0.815	0.183	4.291E-04
Bcl2l11	577.504	-0.757	0.221	1.513E-02
Hpse	372.078	-0.733	0.224	2.444E-02
Tnip1	1882.997	-0.627	0.186	1.857E-02
Irf1	704.821	-0.623	0.201	3.869E-02
B2m	63006.782	-0.517	0.160	2.781E-02
NF-κB family genes				
Nfkbid	152.386	-1.003	0.262	4.317E-03
Nfkbia	768.385	-0.731	0.204	9.368E-03
Nfkb2	2543.102	-0.638	0.197	2.720E-02

baseMean = expression level as indicated by reads across all replicates
log2FoldChange = log2 fold change between the groups; shOPN vs control.
lfcSE = standard error of the log2FoldChange
padj = *P* value adjusted for multiple testing using procedure of Benjamini-Hochberg.
[†]Chemokines not included.
[π] Significant genes only

Supplemental Table 6. Correlations with histological portal inflammation and portal fibrosis in human MASH

Histology	Factor	p-Value[a]	Direction
Portal Inflammation	OPN	0.0006	Positive
Portal Inflammation	CCL2 (MCP1)	0.0012	Positive
Portal Inflammation	IL8	0.0038	Positive
Portal Fibrosis	OPN	0.0008	Positive
Portal Fibrosis	CCL2 (MCP1)	0.0025	Positive
Portal Fibrosis	IL8	0.0001	Positive

[a] Spearman rho, Significant.
Biopsy-proven MASH, scored according to NASH (MASH) CRN [ref 24].
OPN, CCL2 and IL8 detected by Luminex panel, n=123 patients.